
UNDERSTANDING WARMUP-STABLE-DECAY LEARNING RATES: A RIVER VALLEY LOSS LANDSCAPE PERSPECTIVE

Kaiyue Wen Stanford University <code>kaiyuew@stanford.edu</code>	Zhiyuan Li TTIC <code>zhiyuanli@ttic.edu</code>	Jason Wang Stanford University <code>jsywang@stanford.edu</code>
David Hall Stanford University <code>dlwh@cs.stanford.edu</code>	Percy Liang Stanford University <code>pliang@cs.stanford.edu</code>	Tengyu Ma Stanford University <code>tengyuma@cs.stanford.edu</code>

ABSTRACT

Training language models currently requires pre-determining a fixed compute budget because the typical cosine learning rate schedule depends on the total number of steps. In contrast, the Warmup-Stable-Decay (*WSD*) schedule uses a constant learning rate to produce a main branch of iterates that can in principle continue indefinitely without a pre-specified compute budget. Then, given any compute budget, one can branch out from the main branch at a proper at any time with a rapidly decaying learning rate to produce a strong model. Empirically, *WSD* generates an intriguing, non-traditional loss curve: the loss remains elevated during the stable phase but sharply declines during the decay phase. Towards explaining this phenomenon, we conjecture that pretraining loss exhibits a *river valley landscape*, which resembles a deep valley with a river at its bottom. Under this assumption, we show that during the stable phase, the iterate undergoes large oscillations due to the high learning rate, yet it progresses swiftly along the river. During the decay phase, the rapidly dropping learning rate minimizes the iterate’s oscillations, moving it closer to the river and revealing true optimization progress. Therefore, the sustained high learning rate phase and fast decaying phase are responsible for progress in the river and the mountain directions, respectively, and are both critical. Our analysis predicts phenomena consistent with empirical observations and shows that this landscape can naturally emerge from pretraining on a simple bi-gram dataset. Inspired by the theory, we introduce *WSD-S*, a variant of *WSD* that reuses previous checkpoints’ decay phases and keeps only one main branch, where we resume from a decayed checkpoint. *WSD-S* empirically outperforms *WSD* and *Cyclic-Cosine* in obtaining multiple pretrained language model checkpoints across various compute budgets in a single run for parameters scaling from 0.1B to 1.2B.

1 INTRODUCTION

Pre-training large language models (LLMs) typically involves following a learning rate schedule that decreases over a pre-determined number of steps, such as a cosine schedule (Loshchilov & Hutter, 2017; Touvron et al., 2023), where the learning rate starts high and gradually decreases in a smooth curve following the shape of a cosine function. This inflexible approach makes it difficult to adapt to additional compute or data, as the learning rate schedule for all the data is not a natural continuation of the schedule used with past data. Additionally, fitting scaling laws is costly because each compute budget requires retraining to adjust the learning rate schedule (Hoffmann et al., 2022).

In contrast to the cosine learning rate, recent work Hu et al. (2024) introduces the warmup-stable-decay (*WSD*) schedule, which does not require committing to a pre-specified total compute budget. After a standard warm-up period, the *WSD* schedule maintains a main “branch” using a constant

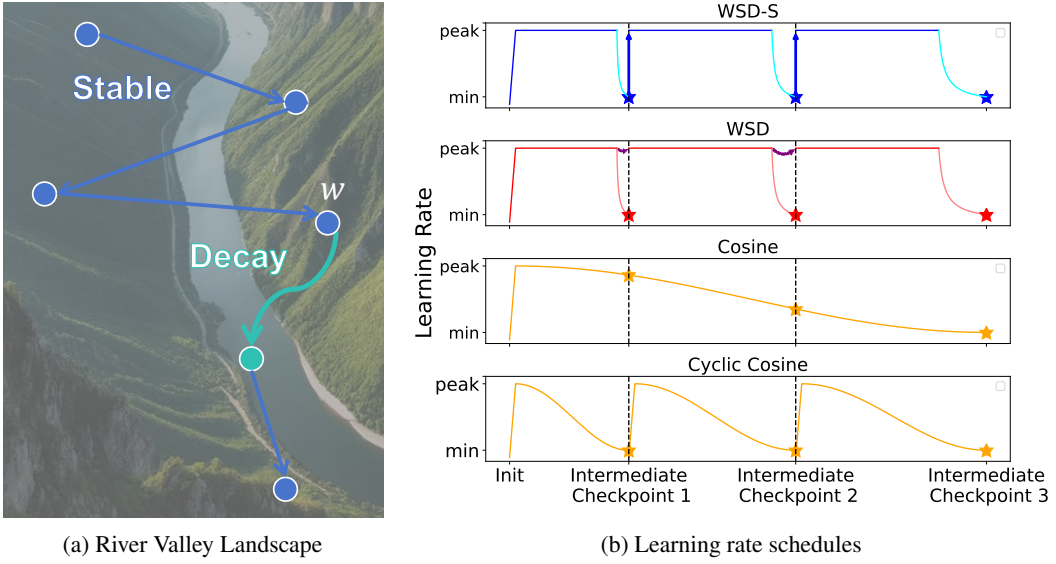


Figure 2: We theoretically analyze the Warmup-Stable-Decay (WSD) schedule and demonstrate a **river valley** loss landscape model to explain its effectiveness (demonstrated in Figure 2a). The stable phase adopts a large learning rate and the iterate will progress along the river while oscillating between the sharp hillsides. Due to the large oscillation caused by the large learning rate, the run will potentially show a higher loss compared to a run using smaller learning rate in this phase. During the decay phase, the learning rate is dropped rapidly to ease the oscillation of the iterates, driving it closer to the river, revealing the optimization progress. Based on our theory, we propose WSD-Simplified (WSD-S), an effective simplification of the WSD schedule in continual learning, where we start directly using a high learning rate from previous intermediate checkpoints. We visualize the learning rate schedule in Figure 2b. The arrow in the second row of Figure 2b indicates WSD reinitializes the checkpoint from the last checkpoint from the constant learning rate phase instead.

learning rate indefinitely and branch off using a fast-decaying learning rate schedule to obtain intermediate checkpoints (see the second row of Figure 2b). Using the WSD schedule, one can continue training from a checkpoint in the main branch by resuming with the same constant learning rate and can obtain training losses for multiple compute budgets with a single run.

Empirically, the WSD schedule produces a non-traditional loss curve (see Figure 1): during the constant learning rate phase, the loss remains higher than the loss using other schedules like the cosine schedule; but during the decay phase, it drops sharply, often leading to a better final performance compared to the cosine schedule. This raises the main question the paper aims to address:

Why does WSD work, especially with such a non-traditional loss curve? Specifically, why does a constant learning rate phase, characterized by slow loss improvements, eventually lead to superior performance?

The first contribution of this paper is a theoretical framework to explain the underlying mechanism of WSD. We characterize a type of loss landscape, called the river valley landscape (Definition 3.1), and theoretically show that WSD has superior performance on such loss landscapes. We show that the river valley landscape can provide multiple theoretical prediction matching the empirical observations and hence can serve as a useful conceptual picture for understanding the pretraining optimization process.

As the name suggests, a river valley landscape intuitively features steeply sloping hillsides with a river winding through the bottom of the gorge (see Figure 2a). During the stochastic gradient-based optimization process, the

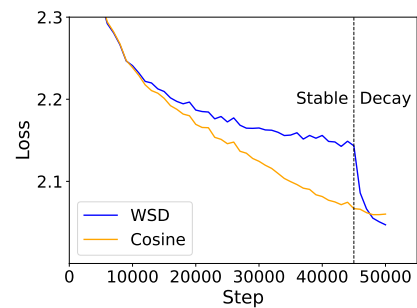


Figure 1: **The Distinctive Loss Curve produced by WSD.** A constant learning rate phase, characterized by slow loss improvements, eventually leads to better validation loss after learning rate decay.

iterate bounces between the hillsides as it slowly and implicitly progresses along the river direction. The loss in this landscape can be decomposed into two components: the *river component*, which represents the primary loss along the river at the bottom of the hills, and the *hill component*, which accounts for the additional loss caused by deviations in height from the river’s course. Progress is determined primarily by the river component in the long run. We demonstrate that when the loss function exhibits this type of landscape, a learning rate schedule should satisfy the following two key properties to effectively minimize the loss.

1. **Sustained high learning rate.** It is advantageous to maintain a large learning rate for as long as possible during training, even at the cost of less reduction in the loss. A large learning rate yields larger bouncing due to the stochasticity of the gradient, increasing the hill component of the loss, but it also makes faster progress in the river direction. In contrast, a small learning rate results in less bouncing, keeping the iterate close to the river, but progress along the river direction is slower. Therefore, a larger learning rate leads to faster fundamental progress minimizing the river component, which is obscured by the oscillation in the hill component. This progress will be revealed by the decay phase discussed below.
2. **Final low learning rate.** As training nears completion, it becomes essential to reduce the learning rate. This decay minimizes the oscillations in the mountain direction to decrease the hill component and ensures that the iterates converge to a point close to the river, which has a lower loss than any nearby points up the mountain.

In Section 3, we provide formal theoretical statements analyzing the trajectories of (stochastic) gradient descent on the river valley landscape, fleshing out the intuitions above. Among our synthetic and real-world studies supporting the river valley landscape hypothesis, an intriguing observation in language model pretraining is that the loss on the linear interpolation of two checkpoints in the stable phase exhibits a convex and unimodal shape, resembling a valley, whereas between two checkpoints in the decay phase, the loss shows a smooth monotone decay.

All the theoretical results above assume a river valley landscape. How likely does the next-token prediction loss follow this pattern, and why? We hypothesize the river valley landscape can naturally arise from the heterogeneity in the stochasticity of different tokens: highly deterministic tokens (which often involve facts and knowledge) contribute to the “river” direction, while uncertain tokens (which often involve flexibility and ambiguity in the language) create the steep hillsides. We demonstrate this insight by showing in Section 4 that under a bigram toy model, indeed the loss has a river valley landscape, and empirically, most properties of the loss curves under various learning rates on the real datasets are still seen in this toy model. We further show that the stable learning rate phase learns the deterministic tokens whereas the decay phase learns better the stochastic tokens.

Finally, we discuss the limitations of *WSD* within our framework and how to go beyond it. In *WSD*, once an intermediate checkpoint is reached, the model and optimizer are rolled back to the end of the stable phase before resuming training with a constant learning rate. However, our theory suggests that the decay phase also contributes to progress along the river direction, so discarding this part of the progress is unnecessary. Moreover, when an organization pretrains an LLM with *WSD*, it needs to release the last checkpoint in a stable-phase to facilitate continual pretraining for another party, adding extra complexity.

To overcome this limitation, we propose a simplified and improved version of *WSD*, called ***WSD-S***, for continual learning. Specifically, *WSD-S* resumes training immediately from the intermediate checkpoint using a high constant learning rate, avoiding the need to roll back to a previous checkpoint.

We evaluate the effectiveness of *WSD-S* with extensive experiments on LLMs from 0.1B to 1.2B parameters in a continual learning setting with 50B, 100B, and 200B tokens as the three target compute budgets. We empirically show that *WSD-S* has performance comparable with independent oracle runs with cosine learning rate schedules optimally tuned on each of the three budgets. Furthermore, *WSD-S* leads to a better validation loss than *WSD* under the same compute budgets due to the re-use of the decay period. We also show through ablation studies that the performance is relatively insensitive to the precise fraction of time spent decaying as long as it is near 10% and the decay does not start shortly after a coincidental loss spike.

2 RELATED WORK

Learning Rate Schedules. Learning rate schedules are crucial in deep learning, with previous studies exploring various options. Smith (2017) was the first to propose a cyclic triangular learning

rate schedule that interleaves decreasing and increasing learning rates. Loshchilov & Hutter (2017) extended the idea to a cyclic cosine learning rate schedule. He et al. (2015) introduced the notion of warmup, which gradually increases the learning rate in the earlier training phase. Goyal et al. (2018); Hoffer et al. (2018); You et al. (2020) concluded that the learning rate should scale linearly with the batch size, which is further theoretically examined in Smith et al. (2020); Li et al. (2021); Malladi et al. (2023). You et al. (2019) performed an analysis on why learning rate schedules are helpful and suspected that the large learning rate at the beginning phase is mostly useful for avoiding memorization of noisy data, which is consistent with our analysis in Section 4.

In the LLM era, works including Hoffmann et al. (2022); DeepSeek-AI et al. (2024); Hu et al. (2024) examined how to choose learning rate schedules for pretraining. In particular, Hu et al. (2024) introduced a learning rate schedule called Warmup-Stable-Decay (*WSD*) that remains constant for the majority of the runs before decaying in language model pretraining, which were studied independently in Zhai et al. (2022); Ibrahim et al. (2024); Hägele et al. (2024). Raffel et al. (2023); Ibrahim et al. (2024) explored another possibility of using an inverse square root schedule to pretrain the language models. Defazio et al. (2023) proposes to use linear decay for the entire training run. Defazio et al. (2024) shows that with appropriate iterate averaging, a constant learning rate schedule can reach better performance than the cosine learning rate schedule. Rae et al. (2022); Gupta et al. (2023); Hu et al. (2024); Ibrahim et al. (2024) examined how to choose a learning rate schedule in a continual learning setting and verified that rewarming-up cosine learning rate brings performance drops that are costly to recover. A common belief is that the performance drop is due to the sudden increase in learning rate during rewarming-up. However, our work shows that increasing the learning rate after a short decay in *WSD* does not cause a similar performance drop as seen with the cosine learning rate, challenging the previous hypothesis. Instead, we suggest that the performance loss associated with rewarming-up cosine learning rate is due to the implicit damage it causes to the model, making it unsuitable for continual training. On the contrast, *WSD* avoids such damage by maintaining a high learning rate during the stable phase, hence the sudden increase in learning rate does not lead to performance drops in continual training.

Continual Learning. Continual learning, the process of updating the model with newly collected data, can improve the models’ knowledge and capability. Previous continual learning research (Aljundi et al., 2019; Veniat et al., 2021; Cossu et al., 2022; Dyer et al., 2022; Harun et al., 2023; Mehta et al., 2023) assumed significant domain shift and aimed to avoid forgetting old knowledge while learning new knowledge. Recent works including Hernandez et al. (2021); Lesort et al. (2023) suggested that optimizers including SGD and Adam have a knowledge accumulation effect and the effect of catastrophic forgetting may be less significant than expected, especially when replay is applied. Our work mainly focuses on continual pre-training without necessarily a strong domain shift and hence does not touch upon the effect of covariance shift. Continual learning is also extensively employed in large language models such as LLaMA to extend their capabilities, such as handling longer contexts (e.g., see Tworkowski et al. (2023); Peng et al. (2023); Chen et al. (2023); Dubey et al. (2024) and references therein) or dealing with new languages and domains (e.g., see Azerbayev et al. (2024); Rozière et al. (2024); Cui et al. (2024) and references therein).

Theoretical Understanding on Loss Landscape. A long line of research aims to better understand the loss landscape in deep learning (e.g., see Freeman & Bruna (2017); Garipov et al. (2018); Li et al. (2020) and references therein). We will highlight several phenomena that are related to our findings.

(1) Ill-conditioned directional sharpness and heavy-tailed noise: Zhang et al. (2020a;b) examined the gradient noise in language modeling and observed that the noise is heavy-tailed in multiple dimensions. Pan & Li (2023); Liu et al. (2024) showed that the loss has vastly different curvatures in different dimensions. Our river valley landscape is consistent with these findings.

(2) Benefit of large learning rates: Large learning rates have a provable regularizing effect in finding flatter minima (Kong & Tao, 2020; Wang et al., 2022), and flatter minima typically have a better generalization effect, even in the pretraining setting (Jiang et al., 2019; Blanc et al., 2020; Liu et al., 2022; Li et al., 2022; Ma et al., 2022; Lyu et al., 2023; Andriushchenko et al., 2023).

(3) Connecting loss landscape with feature learning: Some recent works (Nakkiran et al., 2019; Rosenfeld & Risteski, 2023) tried to understand how the loss landscape is formed through the lens of feature learning. Rosenfeld & Risteski (2023) showed that a large learning rate will cause oscillation in learning subtle classification rules while continuing to learn other more deterministic

features. Wang et al. (2024) studied how to improve generalization and convergence by amplifying the update provided by the optimizer in the flat direction of the loss landscape. Wu et al. (2024); Cai et al. (2024) studied gradient descent dynamics on logistic regression, showing that a large learning rate will cause oscillation in the earlier phase but will lead to higher progress later in training. Pagliardini et al. (2024) developed a modification of the Adam optimizer based on optimization analysis on the Rosenbrock function, which is a special case of the river valley landscape. Song et al. (2024) shows that when SGD update is projected to the dominant subspace of the Hessian, the model’s optimization progress slows down and they conjecture the existence of *ill-conditioned valley* in the landscape, which can be viewed as a similar and simpler version of the river valley landscape discussed in this paper.

The landscape analysis described in these previous works matches our river valley picture at a high level.

3 THEORETICAL ANALYSIS WITH RIVER VALLEY LOSS LANDSCAPES

Intuition and Outline. As illustrated in Figure 3, we will analyze the dynamics of different optimization algorithm on the river valley loss landscape. (1) The **gradient descent (GD)** iterates will quickly converge to the river and track the river afterward (Theorem 3.3). This holds for the continuous limit of GD, gradient flow, as well (Theorem 3.2). (2) Stochastic gradient descent (SGD) algorithm on a river valley loss landscape will bounce between the hillsides due to the noise instead of converging to the river, while still gradually progressing along the river over time (Theorem 3.4). A large learning rate results in significant oscillations but also facilitates rapid advancement in the river’s direction (the **blue** trajectory). Conversely, a small learning rate keeps the iterates closer to the river’s course but leads to slower movement along it (the **yellow** trajectory). While the oscillations in the mountain direction can cause a higher loss for a large learning rate in the short term, the large fundamental progress along the river. (3) Finally, reducing the learning rate before termination (the **cyan** trajectory) helps mitigate these oscillations and reveal the underlying fundamental progress in the river’s direction (Theorem 3.5). In this scenario, the **WSD** algorithm is preferred: the stable phase allows for substantial progress along the river, and the final decay phase reduces oscillations, ensuring that the iterates terminate near the river’s course.

3.1 SETTING AND ASSUMPTIONS

We will now formally present our theory. We use $w \in \mathbb{R}^d$ to denote the parameters and L to denote the loss. Further, we use $\lambda_k(H)$ and $v_k(H)$ to denote the k -th largest eigenvalue and eigenvector of a matrix H , respectively. The “river” in the river valley is a 1-dimensional manifold \mathcal{M} formalized below.

Assumption 1. *We assume the existence of a “river”, which is a 1-dimensional manifold \mathcal{M} such that any point $w \in \mathcal{M}$ has a gradient $\nabla L(w)$ that is in the same direction as the minimal eigenvector direction of the Hessian, $v_d(\nabla^2 L(w))$.*

Under this assumption, at every point on the river, the gradient $\nabla L(w)$ will align with the locally flattest direction, $v_d(\nabla^2 L(w))$, which we refer to as the *river direction*. All other directions orthogonal to the river direction are considered as the *mountain directions*, corresponding to the steep hillsides in our conceptual picture. This definition is illustrated in the 2-dimensional loss landscape shown in Figure 4. In this figure, the **red** line represents the top eigenvector (the sharpest direction), while the **black** line represents the smallest eigenvector (the flattest direction) at each point. Along the **blue** curve, which represents the river, the **orange** negative gradient aligns with the river direction. For a point on the hillside, the negative

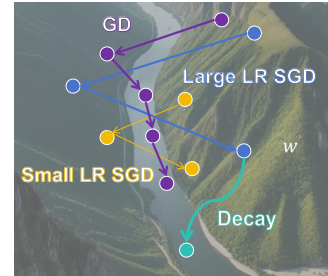


Figure 3: A River Valley Loss Landscape and the Optimization Dynamics with Various Learning Rates.

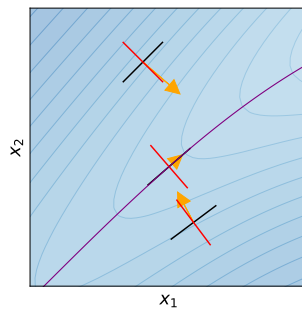


Figure 4: Illustration of the Definition of the River.

gradient pulls the point downward along the hillside towards the river, while also moving it along the river. This intuition will be rigorously formalized in the theorems that follow.

To analyze the optimization dynamics, we will consider a neighborhood U of the river \mathcal{M} . Inside this neighborhood, we will impose several technical assumptions. For example, we will assume that the Hessian has an eigengap between the smallest and the second smallest eigenvalues, so that the river direction is well-defined in U . We will also assume that the last eigenvector of the Hessian v_d changes slowly, which implies that the river direction does not change rapidly during optimization. We summarize these assumptions below.

Assumption 2 (Regularity Assumption). *There exists an open set U containing \mathcal{M} satisfying the following assumptions:*

1. *Analyticity. $L(w)$ is analytic with respect to w .*

2. *Bounded Hessian. There exists a constant $\gamma_{\max} > 0$, such that $\forall w \in U, \|\nabla^2 L(w)\|_{\text{op}} \leq \gamma_{\max}$.*

3. *Existence of Eigengap. There exist constants $\gamma_{\text{flat}}, \gamma > 0$, such that*

$$\forall w \in U, \lambda_{d-1}(\nabla^2 L(w)) > \gamma + 4\gamma_{\text{flat}}, |\lambda_d(\nabla^2 L(w))| < \gamma_{\text{flat}}.$$

4. *Slow Spinning of v_d . There exist constants $\Delta > 0, \kappa \in [0, 0.01)$, such that*

$$\forall w \in U, \Delta_{\min} < \|\nabla L(w)\|_2 \leq \Delta, \text{ and } \|\nabla v_d(\nabla^2 L(w))\|_{\text{op}} \leq \kappa\gamma/(2\Delta).$$

This means that the river direction v_d changes slowly during optimization.

5. *Uniqueness of \mathcal{M} . For any point $w \in U - \mathcal{M}$, the gradient $\nabla L(w)$ is not parallel to $v_d(\nabla^2 L(w))$.*

6. *Conservation of Gradient Flows. There exists an open subset $V \subset U$ and a constant $r > \frac{10\Delta}{\gamma}$ for γ defined in Assumption 2.3 such that $\forall w \in V$, the r -neighborhood of the gradient flow starting from w stays in U for continuous time $T_{\max} \geq 10 \log(2\Delta/(\kappa\Delta_{\min}))/\gamma$.*

Throughout the analysis, κ should be treated as a *small* dimensionless constant, indicating the river spins slowly. We can now define the river valley landscape.

Definition 3.1 (River Valley Landscape). *If a loss function L satisfies Assumptions 1 and 2, then we will claim that the loss function is a river valley.*

One simple example of a river valley landscape is the quadratic loss $L(x_1, x_2) = \frac{\gamma x_1^2}{2} - x_2$ with κ equals to 0. In this case, the river is simply the line $x_2 = 0$. However, the river valley landscape can also be more complex and non-convex, see Figure 3 for an illustration. We will demonstrate that when the loss function is a river valley, the optimization trajectory of (stochastic) gradient descent will track the river. In fact, we can even prove that the iterates will follow the river with a predictable pace, which is characterized by the reference flow defined below.

Reference Flow. We introduce a Riemannian gradient flow constrained to the river \mathcal{M} , serving as a reference in the following theorems. This flow intuitively represents the dynamics of iterates during a gradient flow on the loss constrained by the river. We will denote the projection to the tangential space of the river as $P_{\mathcal{M}}(w)$ for $w \in \mathcal{M}$ and choose an arbitrary starting point x_0 on the river. The reference flow is defined as

$$dx(t) = -P_{\mathcal{M}}(x(t)) \nabla L(x(t)) dt, \quad x(0) = x_0. \quad (1)$$

Here, we use x to represent a point on the river, distinguishing it from w , which denotes a weight in the original space. t refers to the continuous time variable.

3.2 GRADIENT FLOW DYNAMICS

In this section, we will consider gradient flow in the river valley landscape starting from a point $w \in V$, with V defined in Assumption 2.6:

$$dw(t) = -\nabla L(w(t)) dt, \quad w(0) = w \in V. \quad (2)$$

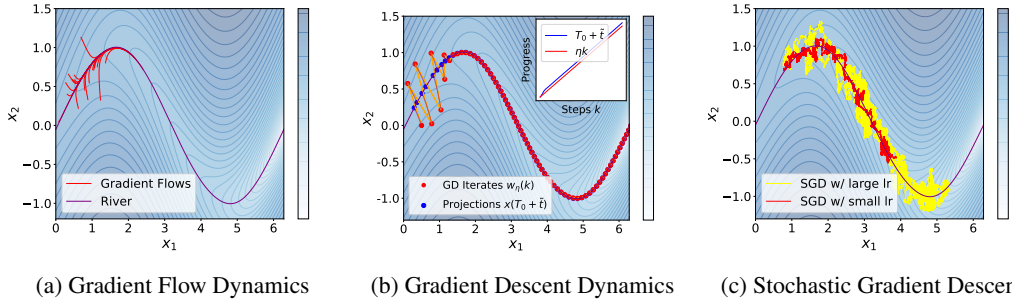


Figure 5: Validation of Theory on a 2D Function. We validate Theorems 3.2 to 3.4 using a 2D example with the loss function $L(x_1, x_2) = (x_2 - \sin(x_1))^2 + 0.2|10 - x_1|$. The blue curve represents the "river", where the gradient aligns with the minimal eigenvector of the Hessian. (1) On the left, we observe that multiple randomly initialized **gradient flows** converge near the river and follow it closely thereafter, consistent with Theorem 3.2. (2) In the middle, we show that discrete gradient descent with a learning rate $\eta = 0.6$ shows similar behavior: after initial oscillations, the **gradient descent iterates** align closely with their **projections** on the river. The inset illustrates that the k -th projection's progress along the reference flow (eq. (1)) approximately equals ηk , as predicted by Theorem 3.3. (3) On the right, we further illustrate that stochastic gradient descent (SGD) also tracks the river. In contrast to the discrete-step gradient descent, the iterates oscillate around the river rather than staying on it. The trajectory with a larger learning rate exhibits both faster progress and greater oscillations compared to the trajectory with a smaller learning rate, as predicted by Theorem 3.4.

We prove in the theorem below that the gradient flow starting from w will eventually converge near the river and remain close to it. Subsequently, if we project the iterate $w(t)$ onto the river, the projection will move along the river at a pace similar to the reference flow $x(\cdot)$ (eq. (1)). This phenomenon is visualized on Figure 5a.

Theorem 3.2. *If a loss L is a river valley (Definition 3.1), for the gradient flow $w(t)$ defined in Equation (2), the iterate will obey the following dynamics:*

1. *The iterate will first converge to a neighborhood of the river. The distance between the iterate and the river is bounded after a constant converge time $T_{\text{converge}} = 2 \log(2\Delta/(\kappa\Delta_{\min}))/\gamma$.*

$$\text{dist}(w(T_{\text{converge}}), \mathcal{M}) = \min_t \|x(t) - w(T_{\text{converge}})\|_2 \leq 2\kappa\Delta/\gamma.$$

2. *After convergence, the iterate will track the river closely with the same pace as the reference flow. There exists a time shift T_0 depending on $w(T_{\text{converge}})$, such that for any $t \in [T_{\text{converge}}, T_{\max}]$ for T_{\max} defined in Assumption 2.6, there exists a $\tilde{t} \in [(1 - \epsilon)T, (1 + \epsilon)T]$ satisfying that,*

$$\|x(T_0 + \tilde{t}) - w(t)\|_2 \leq 2\kappa\Delta/\gamma,$$

for $\epsilon = 30\kappa$.

The proof is deferred to Appendix A.4. In this theorem, the lower bound on T represents the time required for the iterate to converge near the river. Here $x(T_0 + \tilde{t})$ can be viewed as a projection of $w(t)$ onto the river. As both the geometric error ($2\kappa\Delta/\gamma$) and the time-alignment error (ϵ) vanish when κ is small, this projection is not only close to $w(t)$ but also moves at nearly the same rate as the reference flow. Here the term T_0 acts as a shift, reflecting the dependency on the initialization, as optimization trajectories starting from different initial points will enter the river at distinct locations. The term \tilde{t} represents the progress made along the river. This interpretation will remain consistent in the subsequent sections.

Proof Sketch. The proof of Theorem 3.2 relies heavily on the structure of the Hessian matrix. The eigengap assumption (Assumption 2.3) ensures that the loss constrained to the mountain dimensions is steep and convex enough to guarantee convergence to the river. The slow spinning assumption (Assumption 2.4) ensures that the river direction does not change rapidly, allowing the iterate to follow the river closely after convergence.

3.3 GRADIENT DESCENT DYNAMICS

We will now analyze gradient descent with a discrete learning rate. This process is inherently discrete, differentiating it from the continuous gradient flow analyzed above. Similar to the continuous case, an iterate far from the river will converge to the river (as visualized in the first few steps of Figure 5b). To ease our analysis, we will skip the convergence analysis and assume the starting point w lies on the course of the river.

$$w_\eta(k+1) - w_\eta(k) = -\eta \nabla L(w_\eta(k)), \quad w_\eta(0) = w \in \mathcal{M}. \quad (3)$$

Here we use k to denote the discrete time step, in contrast to the continuous time variable t used in the previous section. When the learning rate η is small, despite the discretization error, gradient descent will still track the river closely at approximately the same pace as the reference flow similar to gradient flow. In this case, the progress over k steps will be approximately ηk , as shown in the following theorem.

Theorem 3.3. *If a loss L is a river valley (Definition 3.1), when $\eta < \frac{\gamma}{2\gamma_{\max}^2}$, for the gradient descent $w_\eta(k)$ defined in Equation (3) with initialization w on the river, there exists a time shift T_0 depending on w and η , satisfying that for any $\eta k \leq T_{\max}$, there exists a $\tilde{t} \in [(1-\epsilon)\eta k, (1+\epsilon)\eta k]$ satisfying that,*

$$\|x(T_0 + \tilde{t}) - w_\eta(k)\|_2 \leq 10\kappa\Delta/\gamma,$$

for $\epsilon = 30\kappa + 4\eta\gamma_{\text{flat}}$.

The proof is deferred to Appendix A.5. We observe that the distance of the iterates from the river remains on the same order as in Theorem 3.2. However, the learning rate will affect the pace of the iterates, introducing the additional error term $\eta\gamma_{\text{flat}}$ in time-alignment error (ϵ). This term is unavoidable, as the discretization inherent in gradient descent introduces a slight deviation from the continuous gradient flow, even in the absence of the hill component of the loss. Finally, the Theorem 3.3 predicts that a larger learning rate η will induce higher progress ηk down the river given the same number of steps k .

We illustrate Theorem 3.3 in Figure 5b. Here the **red** points correspond to gradient descent iterates and **green** points are the corresponding predicted projected points on the river. As the theory predicts, the distance between the iterates and projections diminishes after a few steps. Finally, the inset indicates that the projected points traverse the reference flow on the river at a rate proportional to the learning rate η .

3.4 STOCHASTIC GRADIENT DESCENT DYNAMICS

The above analysis holds for deterministic dynamics and we will now proceed to model the stochasticity in the optimization process. This stochasticity will stop the iterate from fully converging to the river and lead to oscillation in the mountain direction. To simplify the analysis, we will consider a special case where the river direction is a constant and the river reduces to a straight line. We conjecture that the results below can be generalized to a more general setup and leave the detailed analysis to future work.

Assumption 3 (Straight River). *For U in Assumption 2, $\forall w \in U, \|\nabla v_d(\nabla^2 L(w))\|_2 = 0$. In this case, the river is a straight line parallel to the direction of $v_d(\nabla^2 L(w))$.*

Under Assumption 3, $v_d(\nabla^2 L(w))$ is a constant vector for $w \in U$ and we will use v_d to denote this vector. We will also assume that the update is deterministic in the direction of the river, which simplifies our proof while still capturing the essential dynamics of SGD. Consequently, we can express the SGD update as follows:

$$\tilde{w}(k+1) = \tilde{w}_k - \eta_k \nabla L(\tilde{w}(k)) + \eta_k g_k, \quad g_k \sim \mathcal{N}(0, \sigma^2 (\mathcal{I}_d - v_d v_d^T)), \quad \tilde{w}(0) = w \in \mathcal{M}. \quad (4)$$

Here $\mathcal{N}(\mu, \Sigma)$ indicates the normal distribution with mean μ and covariance Σ . Compared to deterministic gradient descent, the introduced noise g_k causes the iterates to deviate from the river instead of fully converging to it (see the difference between Figure 5b and Figure 5c). Consequently, we need to impose additional assumptions on the loss landscape to analyze the dynamics of SGD.

Assumption 4 (Regularity Assumption for SGD). *In the setting of Assumptions 2, we assume in addition the following:*

1. *Bounded Hessian. There exists a constant $\tau > 0$, such that for any weight $w \in U$, the nuclear norm of the Hessian is bounded.*

$$\|\nabla^2 L(w)\|_* = \sum_{i=1}^d |\lambda_i(\nabla^2 L(w))| \leq \tau.$$

2. *Bounded Third Order Gradient. There exist constants $\rho > 0, \kappa' \in [0, 0.01]$, such that,*

$$\|\nabla^3 L(w)\|_{\text{op}} \leq \rho, \quad \Delta\rho \leq \kappa'\gamma^2.$$

3. *Bounded Loss. There exists a constant $M > 0$ such that $\forall w, L(w) < M$.*

In this assumption, we treat κ' as a small constant, indicating that the influence of the third-order gradient is minimal. This suggests that the overall shape of the loss landscape is predominantly governed by the first and second-order information. We will now analyze the dynamics of SGD in two phases: the stable phase and the decay phase. In both phases, the iterates will track the reference flow with progress linear to the sum of the learning rates. At the same time, the iterates will also incur a loss due to the noise, which will be linear with respect to the learning rate on the last step.

3.4.1 STABLE PHASE

We start with the stable phase, where the learning rate $\eta_k = \eta$ remains constant. Similar to the deterministic case, we will demonstrate that the expected loss of the iterate $\mathbb{E}[L(\tilde{w}(k))]$ closely follows the loss along the reference flow $L(x(T))$, with $T \approx \eta k$. However, the stochasticity in the updates introduces an additional term, $\eta\sigma^2$, into the loss. This provides a formal basis for decomposing the loss into its river and hill components, that is, $L(x(T))$ and $\eta\sigma^2$, respectively.

Theorem 3.4. *Suppose a loss L is a river valley (Definition 3.1) and satisfies Assumptions 3 and 4. Then, for any constants $\delta \in (0, 1)$, for sufficiently small learning rate η depending on the regularity constants,¹, there exists a time shift T_0 depending on w and η , the SGD iterates (defined in Equation (4)) with $\eta_k = \eta$ satisfies that for any integer $k \in [1/\eta\gamma, T_{\max}/\eta]$, there exists a $\tilde{t} \in [(1 - \epsilon_t)\eta k, (1 + \epsilon_t)\eta k]$ satisfying that,*

$$\mathbb{E}[L(\tilde{w}(k))] - L(x(T_0 + \tilde{t})) = (d - 1)\eta\sigma^2/2 + \epsilon_L$$

where $\epsilon_t = 4\eta\gamma_{\text{flat}}$ and $|\epsilon_L| \leq \tau\eta^2\sigma^2 + \rho(Cd\eta\sigma^2/\gamma)^{3/2} + C\kappa'd\eta\sigma^2 + \delta(2M + \eta\sigma^2d) \ll (d - 1)\eta\sigma^2$ with $C = 200\log(64\gamma T/\delta)$.

The proof is deferred to Appendix A.6. In Theorem 3.4, the error term in the approximation of the pace of the projection remains the same as in the deterministic case (Theorem 3.3). However, the stochasticity introduces an additional hill component $(d - 1)\eta\sigma^2/2$ to the expected loss at the iterate. The hill component increases linearly with the learning rate. The error term in loss term ϵ_L can be decomposed into three parts: (1) $\tau\eta^2\sigma^2 + \rho(C\eta\sigma^2/\gamma)^{3/2}$ are higher order discretization effects of learning rate η ; (2) $C\kappa'd\eta\sigma^2$ is caused by the change of the Hessian in the valley dimensions and will diminish when κ' is small; (3) $\delta(2M + \eta\sigma^2d)$ accounts for the small chances that the iterate will escape the neighborhood of the river due to the stochastic updates. While the theorem only considers the case where v_d is a constant vector, we conjecture that the theorem can be extended to a general setting and verify this conjecture on a toy loss (see Figure 5c).

3.4.2 DECAY PHASE

Finally, we will consider the decay phase in training and will show that a proper decaying schedule can reduce the hill component of the loss rapidly. We will first define our decaying schedule, starting from step $k_s = \lceil T/\eta \rceil$:

$$\eta_k = \frac{\eta}{2 + (k - k_s)\eta\gamma}, \quad k_s \leq k \leq 1.1k_s. \quad (5)$$

¹Deferred to Assumption 7 in Appendix.

We choose this schedule to maximize the loss decrease rate on a quadratic function (see Appendix A.2) because we perform quadratic approximations of the loss near the river in our analysis. Our theorem predicts that the hill component of the loss will decrease linearly with the learning rate under this learning rate schedule, consistent with the empirical findings in Hu et al. (2024).

Theorem 3.5. *Under the setting of Theorem 3.4, the SGD iterates (defined in Equation (4)) with the learning rate schedule defined in Equation (5) satisfies that for any integer $k \in [k_s, 1.1k_s]$, there exists a $\tilde{t} \in [(1 - \epsilon_t)T(k), (1 + \epsilon_t)T(k)]$ satisfying that,*

$$\mathbb{E}[L(\tilde{w}(k))] - L(x(T_0 + \tilde{t})) \leq (d - 1)\eta_k \sigma^2/2 + \epsilon_L$$

$$\text{with } T(k) = T + \sum_{i=k_s}^k \eta_i.$$

The formal proof is deferred to Appendix A.7. Compared with Theorem A.30, the hill component is now dominated by $(d - 1)\eta_k \sigma^2/2$, scaling linearly with the decaying learning rate. When the oscillation level σ is large compared to the loss changes along the river, the loss decrease can then appear faster in the decay phase than in stable phases (see Figure 6). Further, the decaying phase also makes progress along the river, which corresponds to the term $\sum_{i=k_s}^k \eta_i$ in the theorem. Finally, the terms used in our theorem match the scaling law formulation in the concurrent work (Tissue et al., 2024).

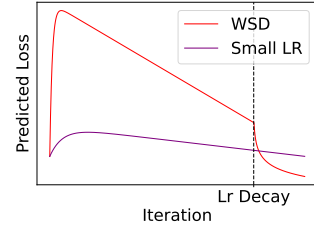


Figure 6: Predicted Loss Curve of SGD By Theorems 3.4 and 3.5 on Loss $L(x_1, x_2) = \gamma x_2^2/2 - x_1$.

3.5 FUTURE EXTENSIONS

We only consider a 1-dimensional river in the theoretical analysis above. However, it is possible to extend our assumptions to a generalized k -dimensional river, where the gradient lies in the flattest k -dimensional subspace for every point on the river.

Assumption 5. *We assume the existence of a “generalized river”, which is a p -dimensional manifold \mathcal{M} such that any point $w \in \mathcal{M}$ has a gradient $\nabla L(w)$ lies in the eigenspace spanned by the last k eigenvectors’ direction of the Hessian, $\{v_i(\nabla^2 L(w)) \mid i \in [d - p + 1, d]\}$.*

Based on this assumption, we can define *generalized river valley Structure*. We believe that under some appropriate assumptions, there will be a similar coupling between the dynamics in the original river valley landscape and the dynamics constrained on the generalized river, and leave this for future work.

There are several other potential technical improvements to our theory that could be explored in future works. First, the analysis of the stochastic setting may be extended to include a river that is not a straight line. Second, the multiplicative constant of 4 in the eigengap condition (Assumption 2.3) might be eliminated through more refined analysis. Lastly, the upper bound on the learning rate in Theorem 3.3 (currently $\gamma/2\gamma_{\max}^2$) could potentially be improved to $\Theta(1/\gamma_{\max})$ through more fine-grained analysis, which is the maximal learning rate in the quadratic case.

3.6 VISUALIZING THE RIVER VALLEY

We use a direct probing method to verify our theory. Our theory suggests that when the learning rate is large, the model will bounce back and forth between the sharp valleys. However, in the decay phase, the model will move downwards the hillside to approach the river. This suggests that if we connect two checkpoints in the stable phase, we should expect to see a projection of the valley, and if we connect two checkpoints in the decay phase, we should expect to see smooth decreasing curves. To verify this, we pretrain a 124M GPT-2 model on OpenWebText. In the first run, we train the model with a constant learning rate for 25B tokens and interpolate between two checkpoints at 20B and 25B tokens (Figure 7a). In the second run, we branch off from the first run at 20B tokens and decay the learning rate for 5B tokens, and we interpolate between two checkpoints at 20B and 25B tokens (Figure 7b). The interpolation results closely resembles our theory. This observation is also

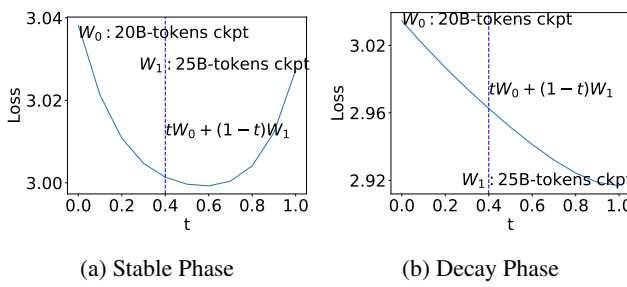


Figure 7: Probing Loss Landscape. We validate the river valley analogy by interpolating stable and decay phases in GPT-2 pretraining experiments. We observe that loss resembles a valley when constrained on the segment connecting two models during the stable phase and smoothly decreases when connecting two models during the decay phase.

consistent with Sanyal et al. (2023) which shows weight averaging improves model performance in the earlier part of the cosine training runs, where the learning rates are higher. Additionally, the smooth decreasing curves we observed when connecting two checkpoints in the decay phase are consistent with the findings in Hägle et al. (2024).

4 UNCERTAINTY VARIATION IN DATA DISTRIBUTION SHAPES THE RIVER VALLEY LANDSCAPE

What causes the loss landscape to resemble a river valley structure? In this section, we propose and validate the hypothesis that variations in next-token uncertainty shape the loss landscape. When predicting a deterministic fact, a large learning rate can boost the model’s confidence, accelerating learning. However, when the next token is inherently ambiguous—such as the continuation of a phrase like “I am”—the model must learn a calibrated distribution, which may necessitate a smaller step size. This variation in uncertainty leads to differences in sharpness across the loss landscape, resulting in the river valley structure.

A Toy Bigram Language. We formalize this intuition using a synthetic language composed of cities and names, where each city corresponds to a unique distribution of its citizens’ names. For instance, one city might have a highly deterministic distribution, with most residents named “Ken”, while another city may have a more diverse distribution of names. This synthetic language follows the structure in Allen-Zhu & Li (2024). The goal is to learn the distribution of names conditioned on each city. We show that cities with more deterministic name distributions align with flatter regions in the loss landscape (the “river”). In contrast, cities with more diverse name distributions correspond to sharper regions (the “hillsides”).

Formally, let the set of cities be represented by $\{1, \dots, n\}$ and the set of names by $\{1, \dots, m\}$. Data is generated by first selecting a city i uniformly at random, then sampling a name j according to the city’s name distribution. The *name distribution* for city i is parameterized by a categorical distribution $\text{Categorical}([P_{i,j}]_{j=1}^m)$, where $P_{i,j}$ represents the probability of selecting name j in city i , and each $P_{i,j} > 0$. To quantify the uncertainty in each city’s name distribution, we compute the Gini impurity of the distribution as:

$$U_i = I_G(\text{name} \mid \text{city} = i) = 1 - \sum_{j=1}^m P_{i,j}^2 \in \left[0, 1 - \frac{1}{m}\right].$$

The value of U_i reflects the uncertainty of city i ’s name distribution. When the distribution is close to deterministic—i.e., there exists a j such that $P_{i,j}$ is near 1— U_i approaches its lower bound of 0. Conversely, for a nearly uniform distribution, U_i approaches its upper bound of $1 - \frac{1}{m}$. Given this setup, we parameterize our model with $\Theta \in \mathbb{R}^{n \times m}$, where each row corresponds to a city and each column to a name. The model estimates the probability of name j for city i using the softmax function $\frac{\exp(\Theta_{i,j})}{\sum_{k=1}^m \exp(\Theta_{i,k})}$.

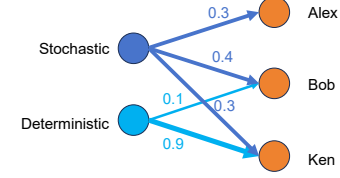


Figure 8: Visualization of Toy Bigram Language. We design a synthetic dataset where each city has a unique name distribution. The left shows the name distributions for two cities, one deterministic and one stochastic.

We use sampled data to train this model. Specifically, for each sampled city i , a name j is drawn according to the true distribution $\mathcal{P}_{i,j}$. The model’s task is to predict the correct name based on the sampled city, minimizing the negative log-likelihood (NLL) over the sampled data. The population loss is given by:

$$L(\Theta) = \frac{1}{n} \sum_{i=1}^n \ell_i(\Theta_{i,:}), \quad \ell_i(\Theta_{i,:}) = - \sum_{j=1}^m \mathcal{P}_{i,j} \log \frac{\exp(\Theta_{i,j})}{\sum_{k=1}^m \exp(\Theta_{i,k})}. \quad (6)$$

This loss is separable across different cities, meaning that the contribution from each city is independent. The loss component $\ell_i(\Theta_{i,:})$ captures the contribution from city i , and different name distributions across cities lead to different forms of ℓ_i . Considering a parameter Θ^* that minimizes the loss L , we will show that cities with more stochastic name distributions correspond to sharper components in the loss landscape, as reflected by the average-direction sharpness of $\ell_i(\text{Tr}(\nabla^2 \ell_i(\theta))|_{\theta=\Theta_{i,:}^*})$.

Lemma 4.1. *The average-direction sharpness of loss component ℓ_i at Θ^* equals the uncertainty of the name distribution (U_i). $\text{Tr}(\nabla^2 \ell_i(\theta))|_{\theta=\Theta_{i,:}^*} = U_i$.*

Lemma 4.1 demonstrates that at the global minimum, the sharpness associated with a city decreases as the city’s name distribution becomes more deterministic. This aligns with the intuition that a deterministic token corresponds to a flatter loss direction.

In a generalized river valley landscape, the hillsides represent the sharper components of the loss, which in this context correspond to cities with more stochastic name distributions. Conversely, the river corresponds to cities with more deterministic name distributions. We can further establish the existence of a generalized river (Assumption 5) in this loss landscape under appropriate assumptions about \mathcal{P} (see Theorem A.33). Along the river, the gradient remains nonzero only for the cities with more deterministic name distributions, reinforcing the connection between determinism and flatness in the loss landscape.

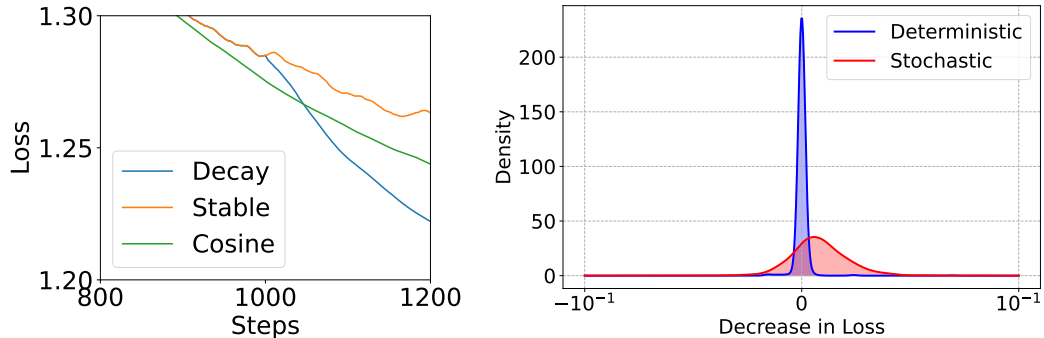


Figure 9: **Loss Curves and Relative Loss Decrease Distribution.** The left figure reproduces the non-traditional loss curve of *WSD* on the synthetic language, showing that the loss remains elevated during the stable phase but sharply declines during the decay phase. The right figure displays the distribution of the relative loss difference from the two different distributions comparing the stable phase and the decay phase. We can observe that the loss decrease over the stochastic distribution is much larger than the decrease in the deterministic distribution.

Empirical Verification. We empirically verify that the loss curve of *WSD* can be reproduced in our synthetic setting. The dataset used contains two types of cities: (1) a deterministic type with name distribution’s entropy less than 0.2, and (2) a stochastic type with name distribution’s entropy greater than 1. Each type contains 1.8k cities and there are 10 possible names. We first train a toy model on this synthetic data and successfully replicate the non-traditional loss curve of *WSD* (Figure 9, left).

Next, we convert the data into a synthetic language in the format "The resident of [CITY]: [NAME]" and fine-tune a GPT-2 model, pretrained on OpenWebText, using this synthetic data. We experiment with two different learning rate schedules: a constant schedule (stable) and a decaying schedule (decay). We then calculate the difference in loss between the two models’ predictions for the first

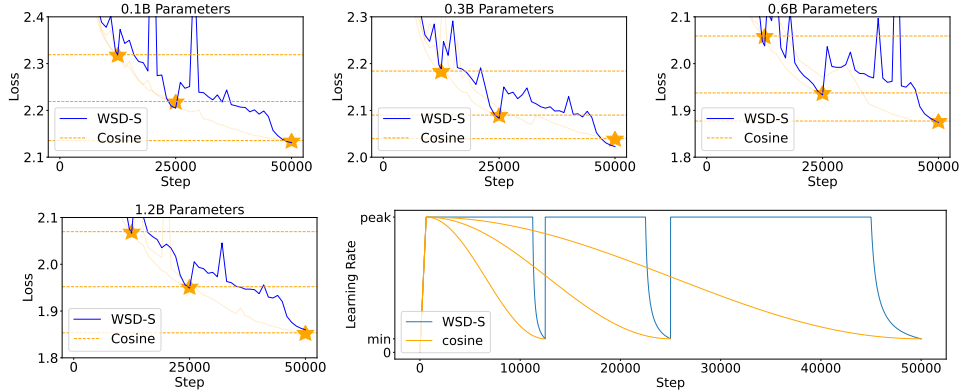


Figure 10: **Comparison with the Cosine Oracles.** We show that the *WSD-S* schedule can perform similarly to the Cosine schedules in a single run. The \star in the graphs visualize the terminating validation loss of different Cosine runs. The largest validation loss gap between the *WSD-S* and the Cosine schedules is $6e-3$. The lower right figure plots the learning rate curves used in this experiment.

token of "[NAME]". A significant Spearman correlation of 0.388 (Figure 9,right) is observed between the loss difference and the ground truth entropy per city. This correlation indicates that the loss decrease is greater during the decay phase for more stochastic populations. Furthermore, although the decay phase achieves a lower overall loss, the mean loss for the deterministic sub-population is slightly higher than in the stable run, suggesting that the stable run better learns the deterministic sub-population.

5 WSD-S: A SIMPLIFICATION OF THE WSD SCHEDULE

5.1 METHOD

The goal of continual pretraining is to generate checkpoints that exhibit good performance at multiple compute budgets in one run. Formally, our goal is to achieve multiple intermediate checkpoints θ_{T_k} , each corresponding to a computing budget (number of steps) T_k for $k \in \{1, \dots, K\}$.

A strong baseline to measure the performance of θ_{T_k} would be running cosine learning rates (Figure 10, lower right) for each budget T_k separately, decays the learning rate linearly to the cosine function between $[0, \pi]$. We will dub this *oracle* method as ***Cosine-Oracle***. However, *Cosine-Oracle* can't be done in a single run and will incur a high total compute budgets $\sum_k T_k$. A simple modification to *Cosine-Oracle* is to use multiple consecutive cosine learning rates between T_{k-1} and T_k (Figure 2b, last row), which we will dub as ***Cyclic-Cosine***. *Cyclic-Cosine* only requires a total compute budgets T_K . However, it leads to non-negligible performance lost compared to *Cosine-Oracle* (Hu et al. (2024)).

Warmup-Stable-Decay (**WSD**) address this issue by maintaining a main branch that keep using a constant learning rate after warmup process and branch off using a decaying learning rate to achieve intermediate checkpoints. One can then continue pretrain from a checkpoint in the main branch by resuming with the same constant learning rate. Formally, *WSD* introduce decay starting points D_1, \dots, D_k such that $T_{i-1} < D_i < T_i$. *WSD* will then correspond to the following process (Figure 2b, second row):

1. Get a main branch of checkpoints θ^{main} by running a constant learning rate schedule for D_K steps.
2. For each k , run a decaying learning rate schedule for $T_k - D_k$ steps starting from $\theta_{D_k}^{\text{main}}$ to get θ_{T_k} .

The above process reutilizes the main branch of checkpoints θ^{main} for each T_k and hence reduces the total compute budget to $T_K + \sum_k (T_k - D_k)$. Recall that in the river valley landscape model, the Warmup-Stable-Decay (**WSD**) algorithm can be viewed as a combination of a large learning

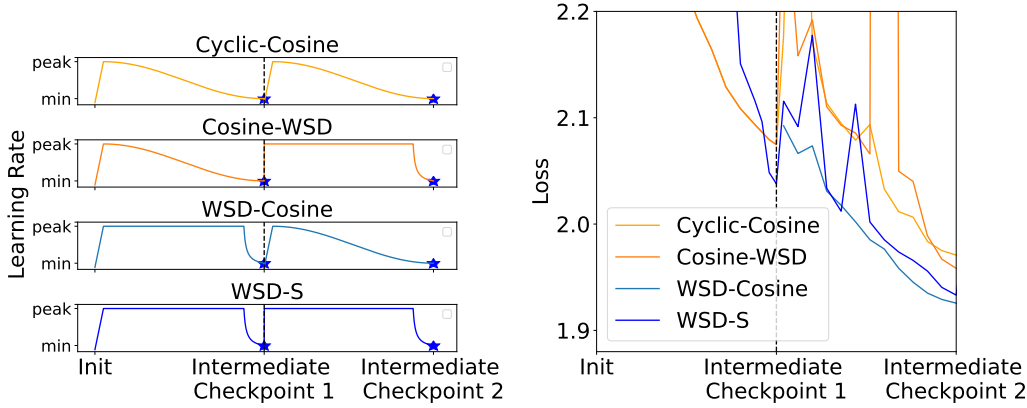


Figure 11: Cosine Learning Rate Implicitly Hurts the Models for Future Continual Learning. We show that while *WSD* and the cosine learning rate schedule may produce similar validation loss in a single run, a model trained with the cosine learning rate schedule is implicitly hurt compared to the model trained with *WSD* for future Continual learning. On the 0.6B models, after training the models for 50B tokens using both *WSD-S* and the cosine learning rate schedule, we continually train two models for another 50B tokens using both learning rates. We observe that the model trained with *WSD-S* consistently outperforms the model trained with the cosine learning rate when used as the starting point for further training.

rate phase to speed up progress down the river and a rapid learning rate drop at the end to reduce the oscillation. Because the decay phase also makes progress along the river (see Theorem 3.5), we propose a simplified version of *WSD*, called Warmup-Stable-Decay-Simplified (***WSD-S***), that continues with another stable phase leaving off of the end of the previous decay phase (see the first row of Figure 2b) without separating the training process into two branches. Formally, the *WSD-S* learning rate schedule is defined as follows:

$$\eta_t = \begin{cases} \text{decay}(T_i - D_i, \eta_{\max}, \eta_{\min})[t - D_i] & \text{if } \exists i, D_i < t \leq T_i; \\ \eta_{\max} & \text{otherwise.} \end{cases} \quad (7)$$

The key difference from our methods is the choice of initialization point when retraining starts. In *WSD*, the second stable phase uses the model before the decay phase, whereas we use the model after it. This process is more convenient to implement because it does not require rolling back to the main branch after each decay phase. Here the learning rate decay function *decay* can take many forms that decay the learning rate from η_{\max} to η_{\min} over $T_i - D_i$ steps. In this paper, we will use the inverse proportional decay function as defined in Equation (8) for all experiments (visualized in Figure 2b, first two rows).

$$\frac{1}{\text{decay}(T, \eta_{\min}, \eta_{\max})} = \left[\frac{t}{T} \frac{1}{\eta_{\min}} + \left(1 - \frac{t}{T}\right) \frac{1}{\eta_{\max}} \mid t \in \{0, 1, \dots, T\} \right]. \quad (8)$$

This function is motivated by the analysis on quadratic functions in Theorem 3.5. The reciprocal of the learning rate linearly interpolates from the reciprocal of maximal to the reciprocal of minimal learning rate.

5.2 EXPERIMENTS

5.2.1 SETUP

Architecture and data. We adopt the LLaMA architecture from Touvron et al. (2023), adjusting the hyperparameters to create four model sizes: 0.1B, 0.3B, 0.6B, and 1.2B. The exact hyperparameters are deferred to Appendix B. These models are trained on the Pile dataset (Gao et al., 2020) with a context length of 4096 and a batch size of 4M tokens.

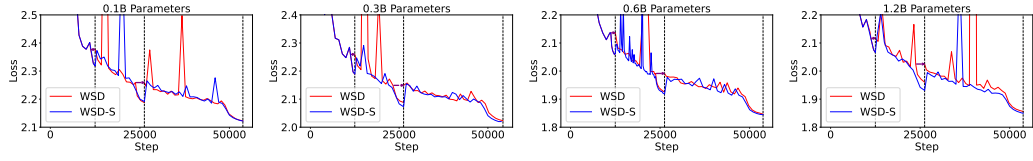


Figure 12: **Comparison With WSD.** We show that *WSD-S* performs favorably compared with *WSD* when the total computes is fixed, achieving a consistent improvement over *WSD* on all the model sizes when trained for approximately 200B tokens.

Implementation. We set the batch size to 1024 and fixed the peak learning rate for the same model size for all the methods. For the 0.1B and 0.3B models, we use a peak learning rate of 6e-4, and for the 0.6B and 1.2B models, we use a peak learning rate of 4e-4. These values are chosen following current empirical practice (e.g. see Groeneveld et al. (2024)). We set the minimal learning rate to 0.1 of the peak learning rate. We use a TPU v3-256 model to train the model with the Levanter framework in Jax (Bradbury et al., 2018; CRFM, 2024). The fraction of time spent decaying is chosen to be 10%. The only exception is that when running *WSD* on the 0.3B models, we encounter a loss spike after training for 22.5B tokens and decay at the checkpoint trained for 22B tokens instead. This change is in favor of *WSD* in our comparison between *WSD-S* and *WSD*. The detailed hyperparameters are deferred to Appendix B.

5.2.2 RESULTS

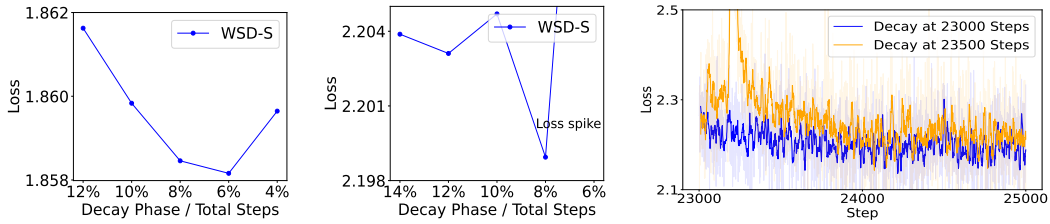
WSD-S performs competitively with *Cosine-Oracle*. The three endpoints of *WSD-S* are set at 50B, 100B, and 200B tokens for all models. As shown in Figure 10, *WSD-S* delivers competitive results compared to *Cosine-Oracle* in a single run.

WSD-S significantly outperforms *Cyclic-Cosine*. We compare the *Cyclic-Cosine* and the *WSD-S* on 0.6B models with a total token budget of 100B tokens. Both schedules reduce to a minimal learning rate at 50B tokens to obtain an intermediate checkpoint. Our results show that *WSD-S* outperforms *Cyclic-Cosine* with a significant performance gap of 4e-2 (Figure 11). A common belief is that loss spiking after increasing the learning rate is the main cause of the performance loss in *Cyclic-Cosine*. However, this belief does not explain the advantage of *WSD-S*. We hypothesize that a model trained with a small learning rate for too long, as with *Cosine*, is implicitly hurt compared to a model trained with a large learning rate for the majority of the run, as with *WSD* or *WSD-S*.

To show that the model trained with *WSD* is more suitable for continual training, we conducted ablation studies by interchanging the schedules in the latter half of the runs to create two new learning rates (*Cosine-WSD* and *WSD-Cosine*). Among the four runs, the model trained using *WSD* for the first half consistently achieved lower loss in continual learning, indicating that *WSD* produces models more suitable for continual learning, even after learning rate decay.

WSD-S matches (and slightly outperforms) *WSD* given the same total compute. For *WSD*, we adopt the following comparison methodology: assuming a 10% decay portion, to get three checkpoints at 12.5k, 25k, and 50k steps, *WSD* then requires corresponding total steps of 12.5k, 26.25k, and 53.75k. Hence, we examine whether *WSD-S* can output three models of matching or better performance in the same corresponding steps (see Figure 12). Our results suggest that *WSD-S* consistently outperforms *WSD* when trained on 200B tokens and underperforms *WSD* only on the smallest scale experiments when we trained 0.1B models for 25k steps. As this is the smallest scale experiment, we conclude that *WSD-S* has a slight advantage over *WSD* when the total compute is fixed. This matches our intuition that *WSD-S* can reuse the decay phases of previous checkpoints, leading to a more efficient use of the total compute. As a simpler version of *WSD*, *WSD-S* is more user-friendly for open-source pretrained models, allowing users to continue training the final checkpoint without needing intermediate ones given that the pretrained models are trained with *WSD* or *WSD-S*.

WSD and WSD-S is not sensitive to the fraction of time spent decaying We conclude with an ablation study on the fraction of time spent decaying, and the result is shown in Figure 13. The final performance matches tightly within the range of 8% to 12%, showing small sensitivity to the choice of the decay portion.



(a) 1.2B Models on 200B tokens (b) 0.1B Models on 100B tokens (c) 0.1B Models on 100B Tokens. Decay Near a Loss Spike (6%)

Figure 13: **Ablation Study on the Sensitivity of Fraction of Time Decaying.** This study examines two settings: a smaller scale with 0.1B parameters trained on 100B tokens (middle figure) and a larger scale with 0.6B parameters trained on 200B tokens (left figure). The results indicate that the final performance is similar when the decay phase is 8%-12% of the total training steps. However, the right figure demonstrates a significant performance loss when decaying near a loss spike. It compares two training loss curves with decay phases of 8% and 6% of the total compute on the 0.1B models, where the latter starts immediately after a loss spike, leading to a validation loss increase of 2e-2.

However, in our experiments, we observe that decaying near a loss spike can lead to a significant performance loss (Figure 13, right). With the large learning rate, the training runs tend to be very volatile and there are multiple loss spikes in the training (see Figure 10). If a decay happens closely *after* a loss spike and the loss has not yet decreased to its original level, it is typical that the final validation loss will be worse by 1e-2 or even more. We observe the same phenomenon for *WSD*, and when such a scenario happens, we suggest either running longer till the loss stabilizes or rolling back to a slightly earlier checkpoint before the loss spikes and decays from there.

6 CONCLUSION

In this work, we propose a river valley landscape metaphor to explain why large learning rates can make implicit progress in training that can only be revealed when the learning rate is decayed. Further, we propose a simple data model that can generate the river valley landscape, attributing the difference of sharpness in different directions to the difference in uncertainty between different tokens. Based on our theory, we propose a learning rate schedule called *WSD-S* that can produce multiple intermediate checkpoints in a single-consecutive run as good as if we prespecified the individual budgets and used a tuned cosine learning rate. The learning rate schedule involves rapidly decaying to a minimal learning rate level at these budgets and resuming to a high constant learning rate immediately afterward and keeping the learning rate constant in the rest of the runs. From training language models from 0.1B to 1.2B parameters, we show *WSD-S* performs competitively with cosine learning rate and outperforms other compute-agnostic learning rates including *WSD* and cyclic-cosine learning rate fixing the total compute budget.

ACKNOWLEDGEMENT

The authors would like to thank the support of NSF 2211780.

REFERENCES

Rahaf Aljundi, Lucas Caccia, Eugene Belilovsky, Massimo Caccia, Min Lin, Laurent Charlin, and Tinne Tuytelaars. Online continual learning with maximally interfered retrieval, 2019.

Zeyuan Allen-Zhu and Yuanzhi Li. Physics of language models: Part 3.3, knowledge capacity scaling laws, 2024. URL <https://arxiv.org/abs/2404.05405>.

Maksym Andriushchenko, Aditya Varre, Loucas Pillaud-Vivien, and Nicolas Flammarion. Sgd with large step sizes learns sparse features, 2023. URL <https://arxiv.org/abs/2210.05337>.

Zhangir Azerbayev, Hailey Schoelkopf, Keiran Paster, Marco Dos Santos, Stephen McAleer, Albert Q. Jiang, Jia Deng, Stella Biderman, and Sean Welleck. Llemma: An open language model for mathematics, 2024. URL <https://arxiv.org/abs/2310.10631>.

Guy Blanc, Neha Gupta, Gregory Valiant, and Paul Valiant. Implicit regularization for deep neural networks driven by an ornstein-uhlenbeck like process, 2020.

James Bradbury, Roy Frostig, Peter Hawkins, Matthew James Johnson, Chris Leary, Dougal Maclaurin, George Necula, Adam Paszke, Jake VanderPlas, Skye Wanderman-Milne, and Qiao Zhang. JAX: composable transformations of Python+NumPy programs, 2018. URL <http://github.com/google/jax>.

Yuhang Cai, Jingfeng Wu, Song Mei, Michael Lindsey, and Peter L. Bartlett. Large stepsize gradient descent for non-homogeneous two-layer networks: Margin improvement and fast optimization, 2024. URL <https://arxiv.org/abs/2406.08654>.

Shouyuan Chen, Sherman Wong, Liangjian Chen, and Yuandong Tian. Extending context window of large language models via positional interpolation, 2023. URL <https://arxiv.org/abs/2306.15595>.

Andrea Cossu, Tinne Tuytelaars, Antonio Carta, Lucia Passaro, Vincenzo Lomonaco, and Davide Bacciu. Continual pre-training mitigates forgetting in language and vision, 2022.

Stanford CRFM. Levanter. <https://github.com/stanford-crfm/levanter>, 2024.

Yiming Cui, Ziqing Yang, and Xin Yao. Efficient and effective text encoding for chinese llama and alpaca, 2024. URL <https://arxiv.org/abs/2304.08177>.

DeepSeek-AI, :, Xiao Bi, Deli Chen, Guanting Chen, Shanhuang Chen, Damai Dai, Chengqi Deng, Honghui Ding, Kai Dong, Qiushi Du, Zhe Fu, Huazuo Gao, Kaige Gao, Wenjun Gao, Ruiqi Ge, Kang Guan, Daya Guo, Jianzhong Guo, Guangbo Hao, Zhewen Hao, Ying He, Wenjie Hu, Panpan Huang, Erhang Li, Guowei Li, Jiashi Li, Yao Li, Y. K. Li, Wenfeng Liang, Fangyun Lin, A. X. Liu, Bo Liu, Wen Liu, Xiaodong Liu, Xin Liu, Yiyuan Liu, Haoyu Lu, Shanghao Lu, Fuli Luo, Shirong Ma, Xiaotao Nie, Tian Pei, Yishi Piao, Junjie Qiu, Hui Qu, Tongzheng Ren, Zehui Ren, Chong Ruan, Zhangli Sha, Zhihong Shao, Junxiao Song, Xuecheng Su, Jingxiang Sun, Yaofeng Sun, Minghui Tang, Bingxuan Wang, Peiyi Wang, Shiyu Wang, Yaohui Wang, Yongji Wang, Tong Wu, Y. Wu, Xin Xie, Zhenda Xie, Ziwei Xie, Yiliang Xiong, Hanwei Xu, R. X. Xu, Yanhong Xu, Dejian Yang, Yuxiang You, Shuiping Yu, Xingkai Yu, B. Zhang, Haowei Zhang, Lecong Zhang, Liyue Zhang, Mingchuan Zhang, Minghua Zhang, Wentao Zhang, Yichao Zhang, Chenggang Zhao, Yao Zhao, Shangyan Zhou, Shunfeng Zhou, Qihao Zhu, and Yuheng Zou. Deepseek llm: Scaling open-source language models with longtermism, 2024.

Aaron Defazio, Ashok Cutkosky, Harsh Mehta, and Konstantin Mishchenko. When, why and how much? adaptive learning rate scheduling by refinement, 2023. URL <https://arxiv.org/abs/2310.07831>.

Aaron Defazio, Xingyu Alice Yang, Harsh Mehta, Konstantin Mishchenko, Ahmed Khaled, and Ashok Cutkosky. The road less scheduled, 2024. URL <https://arxiv.org/abs/2405.15682>.

Abhimanyu Dubey, Abhinav Jauhri, Abhinav Pandey, Abhishek Kadian, Ahmad Al-Dahle, Aiesha Letman, Akhil Mathur, Alan Schelten, Amy Yang, Angela Fan, Anirudh Goyal, Anthony Hartshorn, Aobo Yang, Archi Mitra, Archie Sravankumar, Artem Korenev, Arthur Hinsvark, Arun Rao, Aston Zhang, Aurelien Rodriguez, Austen Gregerson, Ava Spataru, Baptiste Roziere, Bethany Biron, Bin Tang, Bobbie Chern, Charlotte Caucheteux, Chaya Nayak, Chloe Bi, Chris Marra, Chris McConnell, Christian Keller, Christophe Touret, Chunyang Wu, Corinne Wong, Cristian Canton Ferrer, Cyrus Nikolaidis, Damien Allonsius, Daniel Song, Danielle Pintz, Danny Livshits, David Esiobu, Dhruv Choudhary, Dhruv Mahajan, Diego Garcia-Olano, Diego Perino, Dieuwke Hupkes, Egor Lakomkin, Ehab AlBadawy, Elina Lobanova, Emily Dinan, Eric Michael Smith, Filip Radenovic, Frank Zhang, Gabriel Synnaeve, Gabrielle Lee, Georgia Lewis Anderson, Graeme Nail, Gregoire Mialon, Guan Pang, Guillem Cucurell, Hailey Nguyen, Hannah Korevaar, Hu Xu, Hugo Touvron, Iliyan Zarov, Imanol Arrieta Ibarra, Isabel Kloumann, Ishan Misra, Ivan Evtimov, Jade Copet, Jaewon Lee, Jan Geffert, Jana Vranes, Jason Park, Jay Mahadeokar, Jeet Shah, Jelmer van der Linde, Jennifer Billock, Jenny Hong, Jena Lee, Jeremy Fu, Jianfeng Chi, Jianyu Huang, Jiawen Liu, Jie Wang, Jiecao Yu, Joanna Bitton, Joe Spisak, Jongsoo Park, Joseph Rocca, Joshua Johnstun, Joshua Saxe, Junteng Jia, Kalyan Vasudevan Alwala, Kartikeya Upasani, Kate Plawiak, Ke Li, Kenneth Heafield, Kevin Stone, Khalid El-Arini, Krithika Iyer, Kshitiz Malik, Kuenley Chiu, Kunal Bhalla, Lauren Rantala-Yeary, Laurens van der Maaten, Lawrence Chen, Liang Tan, Liz Jenkins, Louis Martin, Lovish Madaan, Lubo Malo, Lukas Blecher, Lukas Landzaat, Luke de Oliveira, Madeline Muzzi, Mahesh Pasupuleti, Mannat Singh, Manohar Paluri, Marcin Kardas, Mathew Oldham, Mathieu Rita, Maya Pavlova, Melanie Kambadur, Mike Lewis, Min Si, Mitesh Kumar Singh, Mona Hassan, Naman Goyal, Narjes Torabi, Nikolay Bashlykov, Nikolay Bogoychev, Niladri Chatterji, Olivier Duchenne, Onur Çelebi, Patrick Alrassy, Pengchuan Zhang, Pengwei Li, Petar Vasic, Peter Weng, Prajwal Bhargava, Pratik Dubal, Praveen Krishnan, Punit Singh Koura, Puxin Xu, Qing He, Qingxiao Dong, Ragavan Srinivasan, Raj Ganapathy, Ramon Calderer, Ricardo Silveira Cabral, Robert Stojnic, Roberta Raileanu, Rohit Girdhar, Rohit Patel, Romain Sauvestre, Ronnie Polidoro, Roshan Sumbaly, Ross Taylor, Ruan Silva, Rui Hou, Rui Wang, Saghar Hosseini, Sahana Chennabasappa, Sanjay Singh, Sean Bell, Seohyun Sonia Kim, Sergey Edunov, Shaoliang Nie, Sharan Narang, Sharath Raparthy, Sheng Shen, Shengye Wan, Shruti Bhosale, Shun Zhang, Simon Vandenhende, Soumya Batra, Spencer Whitman, Sten Sootla, Stephane Collot, Suchin Gururangan, Sydney Borodinsky, Tamar Herman, Tara Fowler, Tarek Sheasha, Thomas Georgiou, Thomas Scialom, Tobias Speckbacher, Todor Mihaylov, Tong Xiao, Ujjwal Karn, Vedanuj Goswami, Vibhor Gupta, Vignesh Ramanathan, Viktor Kerkez, Vincent Gonguet, Virginie Do, Vish Vogeti, Vladan Petrovic, Weiwei Chu, Wenhan Xiong, Wenyin Fu, Whitney Meers, Xavier Martinet, Xiaodong Wang, Xiaoqing Ellen Tan, Xinfeng Xie, Xuchao Jia, Xuewei Wang, Yaelle Goldschlag, Yashesh Gaur, Yasmine Babaei, Yi Wen, Yiwen Song, Yuchen Zhang, Yue Li, Yuning Mao, Zacharie Delpierre Coudert, Zheng Yan, Zhengxing Chen, Zoe Papakipos, Aaditya Singh, Aaron Grattafiori, Abha Jain, Adam Kelsey, Adam Shajnfeld, Adithya Gangidi, Adolfo Victoria, Ahuva Goldstand, Ajay Menon, Ajay Sharma, Alex Boesenberg, Alex Vaughan, Alexei Baevski, Allie Feinstein, Amanda Kallet, Amit Sangani, Anam Yunus, Andrei Lupu, Andres Alvarado, Andrew Caples, Andrew Gu, Andrew Ho, Andrew Poulton, Andrew Ryan, Ankit Ramchandani, Annie Franco, Aparajita Saraf, Arkabandhu Chowdhury, Ashley Gabriel, Ashwin Bharambe, Assaf Eisenman, Azadeh Yazdan, Beau James, Ben Maurer, Benjamin Leonhardi, Bernie Huang, Beth Loyd, Beto De Paola, Bhargavi Paranjape, Bing Liu, Bo Wu, Boyu Ni, Braden Hancock, Bram Wasti, Brandon Spence, Brani Stojkovic, Brian Gamido, Britt Montalvo, Carl Parker, Carly Burton, Catalina Mejia, Changhan Wang, Changkyu Kim, Chao Zhou, Chester Hu, Ching-Hsiang Chu, Chris Cai, Chris Tindal, Christoph Feichtenhofer, Damon Civin, Dana Beaty, Daniel Kreymer, Daniel Li, Danny Wyatt, David Adkins, David Xu, Davide Testuggine, Delia David, Devi Parikh, Diana Liskovich, Didem Foss, Dingkang Wang, Duc Le, Dustin Holland, Edward Dowling, Eissa Jamil, Elaine Montgomery, Eleonora Presani, Emily Hahn, Emily Wood, Erik Brinkman, Esteban Arcaute, Evan Dunbar, Evan Smothers, Fei Sun, Felix Kreuk, Feng Tian, Firat Ozgenel, Francesco Caggioni, Francisco Guzmán, Frank Kanayet, Frank Seide, Gabriela Medina Florez, Gabriella Schwarz, Gada Badeer, Georgia Swee, Gil Halpern, Govind Thattai, Grant Herman, Grigory Sizov, Guangyi, Zhang, Guna Lakshminarayanan, Hamid Shojanazeri, Han Zou, Hannah Wang, Hanwen Zha, Haroun Habeeb, Harrison Rudolph, Helen Suk, Henry Aspegren, Hunter Goldman, Ibrahim Damlaj, Igor Molybog, Igor Tufanov, Irina-Elena Veliche, Itai Gat, Jake Weissman, James Geboski, James Kohli, Japhet Asher, Jean-Baptiste Gaya, Jeff Marcus, Jeff Tang, Jennifer Chan, Jenny Zhen, Jeremy Reizenstein, Jeremy Teboul, Jessica Zhong, Jian Jin, Jingyi Yang, Joe Cummings, Jon Carvill, Jon Shepard, Jonathan McPhie,

Jonathan Torres, Josh Ginsburg, Junjie Wang, Kai Wu, Kam Hou U, Karan Saxena, Karthik Prasad, Kartikay Khandelwal, Katayoun Zand, Kathy Matosich, Kaushik Veeraraghavan, Kelly Michelena, Keqian Li, Kun Huang, Kunal Chawla, Kushal Lakhota, Kyle Huang, Lailin Chen, Lakshya Garg, Lavender A, Leandro Silva, Lee Bell, Lei Zhang, Liangpeng Guo, Licheng Yu, Liron Moshkovich, Luca Wehrstedt, Madian Khabsa, Manav Avalani, Manish Bhatt, Maria Tsimpoukelli, Martynas Mankus, Matan Hasson, Matthew Lennie, Matthias Reso, Maxim Groshev, Maxim Naumov, Maya Lathi, Meghan Keneally, Michael L. Seltzer, Michal Valko, Michelle Restrepo, Mihir Patel, Mik Vyatskov, Mikayel Samvelyan, Mike Clark, Mike Macey, Mike Wang, Miquel Jubert Hermoso, Mo Metanat, Mohammad Rastegari, Munish Bansal, Nandhini Santhanam, Natascha Parks, Natasha White, Navyata Bawa, Nayan Singhal, Nick Egebo, Nicolas Usunier, Nikolay Pavlovich Laptev, Ning Dong, Ning Zhang, Norman Cheng, Oleg Chernoguz, Olivia Hart, Omkar Salpekar, Ozlem Kalinli, Parkin Kent, Parth Parekh, Paul Saab, Pavan Balaji, Pedro Rittner, Philip Bontrager, Pierre Roux, Piotr Dollar, Polina Zvyagina, Prashant Ratanchandani, Pritish Yuvaraj, Qian Liang, Rachad Alao, Rachel Rodriguez, Rafi Ayub, Raghatham Murthy, Raghu Nayani, Rahul Mitra, Raymond Li, Rebekkah Hogan, Robin Battey, Rocky Wang, Rohan Maheswari, Russ Howes, Ruty Rinott, Sai Jayesh Bondu, Samyak Datta, Sara Chugh, Sara Hunt, Sargun Dhillon, Sasha Sidorov, Satadru Pan, Saurabh Verma, Seiji Yamamoto, Sharadh Ramaswamy, Shaun Lindsay, Shuang Zhang, Shuang Zhang, Sinong Wang, Sneha Agarwal, Soji Sajuyigbe, Soumith Chintala, Stephanie Max, Stephen Chen, Steve Kehoe, Steve Satterfield, Sudarshan Govindaprasad, Sumit Gupta, Sungmin Cho, Sunny Virk, Suraj Subramanian, Sy Choudhury, Sydney Goldman, Tal Remez, Tamar Glaser, Tamara Best, Thilo Kohler, Thomas Robinson, Tianhe Li, Tianjun Zhang, Tim Matthews, Timothy Chou, Tzook Shaked, Varun Vontimitta, Victoria Ajayi, Victoria Montanez, Vijai Mohan, Vinay Satish Kumar, Vishal Mangla, Vitor Albiero, Vlad Ionescu, Vlad Poenaru, Vlad Tiberiu Mihailescu, Vladimir Ivanov, Wei Li, Wenchen Wang, Wenwen Jiang, Wes Bouaziz, Will Constable, Xiaocheng Tang, Xiaofang Wang, Xiaojian Wu, Xiaolan Wang, Xide Xia, Xilun Wu, Xinbo Gao, Yanjun Chen, Ye Hu, Ye Jia, Ye Qi, Yenda Li, Yilin Zhang, Ying Zhang, Yossi Adi, Youngjin Nam, Yu, Wang, Yuchen Hao, Yundi Qian, Yuzi He, Zach Rait, Zachary DeVito, Zef Rosnbrick, Zhaoduo Wen, Zhenyu Yang, and Zhiwei Zhao. The llama 3 herd of models, 2024. URL <https://arxiv.org/abs/2407.21783>.

Ethan Dyer, Aitor Lewkowycz, and Vinay Ramasesh. Effect of scale on catastrophic forgetting in neural networks. In *ICLR*, 2022. URL https://openreview.net/forum?id=GhVS8_yPeEa.

K. J. Falconer. Differentiation of the limit mapping in a dynamical system. *Journal of the London Mathematical Society*, s2-27(2):356–372, 1983. doi: 10.1112/jlms/s2-27.2.356. URL <https://academic.oup.com/jlms/article-abstract/s2-27/2/356/814475>.

C. Daniel Freeman and Joan Bruna. Topology and geometry of half-rectified network optimization, 2017. URL <https://arxiv.org/abs/1611.01540>.

Leo Gao, Stella Biderman, Sid Black, Laurence Golding, Travis Hoppe, Charles Foster, Jason Phang, Horace He, Anish Thite, Noa Nabeshima, Shawn Presser, and Connor Leahy. The pile: An 800gb dataset of diverse text for language modeling, 2020.

Timur Garipov, Pavel Izmailov, Dmitrii Podoprikhin, Dmitry Vetrov, and Andrew Gordon Wilson. Loss surfaces, mode connectivity, and fast ensembling of dnns, 2018. URL <https://arxiv.org/abs/1802.10026>.

Priya Goyal, Piotr Dollár, Ross Girshick, Pieter Noordhuis, Lukasz Wesolowski, Aapo Kyrola, Andrew Tulloch, Yangqing Jia, and Kaiming He. Accurate, large minibatch sgd: Training imagenet in 1 hour, 2018.

Dirk Groeneveld, Iz Beltagy, Pete Walsh, Akshita Bhagia, Rodney Kinney, Oyvind Tafjord, Ananya Harsh Jha, Hamish Ivison, Ian Magnusson, Yizhong Wang, Shane Arora, David Atkinson, Russell Author, Khyathi Raghavi Chandu, Arman Cohan, Jennifer Dumas, Yanai Elazar, Yuling Gu, Jack Hessel, Tushar Khot, William Merrill, Jacob Morrison, Niklas Muennighoff, Aakanksha Naik, Crystal Nam, Matthew E. Peters, Valentina Pyatkin, Abhilasha Ravichander, Dustin Schwenk, Saurabh Shah, Will Smith, Emma Strubell, Nishant Subramani, Mitchell Wortsman, Pradeep

Dasigi, Nathan Lambert, Kyle Richardson, Luke Zettlemoyer, Jesse Dodge, Kyle Lo, Luca Soldaini, Noah A. Smith, and Hannaneh Hajishirzi. Olmo: Accelerating the science of language models, 2024. URL <https://arxiv.org/abs/2402.00838>.

Kshitij Gupta, Benjamin Thérien, Adam Ibrahim, Mats L. Richter, Quentin Anthony, Eugene Belilovsky, Irina Rish, and Timothée Lesort. Continual pre-training of large language models: How to (re)warm your model?, 2023.

Md Yousuf Harun, Jhair Gallardo, Tyler L. Hayes, Ronald Kemker, and Christopher Kanan. Siesta: Efficient online continual learning with sleep, 2023.

Kaiming He, Xiangyu Zhang, Shaoqing Ren, and Jian Sun. Deep residual learning for image recognition, 2015.

Danny Hernandez, Jared Kaplan, Tom Henighan, and Sam McCandlish. Scaling laws for transfer, 2021.

Elad Hoffer, Itay Hubara, and Daniel Soudry. Train longer, generalize better: closing the generalization gap in large batch training of neural networks, 2018.

Jordan Hoffmann, Sebastian Borgeaud, Arthur Mensch, Elena Buchatskaya, Trevor Cai, Eliza Rutherford, Diego de Las Casas, Lisa Anne Hendricks, Johannes Welbl, Aidan Clark, Tom Hennigan, Eric Noland, Katie Millican, George van den Driessche, Bogdan Damoc, Aurelia Guy, Simon Osindero, Karen Simonyan, Erich Elsen, Jack W. Rae, Oriol Vinyals, and Laurent Sifre. Training compute-optimal large language models, 2022.

Shengding Hu, Yuge Tu, Xu Han, Chaoqun He, Ganqu Cui, Xiang Long, Zhi Zheng, Yewei Fang, Yuxiang Huang, Weilin Zhao, Xinrong Zhang, Zheng Leng Thai, Kaihuo Zhang, Chongyi Wang, Yuan Yao, Chenyang Zhao, Jie Zhou, Jie Cai, Zhongwu Zhai, Ning Ding, Chao Jia, Guoyang Zeng, Dahai Li, Zhiyuan Liu, and Maosong Sun. Minicpm: Unveiling the potential of small language models with scalable training strategies, 2024.

Alexander Hägele, Elie Bakouch, Atli Kosson, Loubna Ben Allal, Leandro Von Werra, and Martin Jaggi. Scaling laws and compute-optimal training beyond fixed training durations, 2024. URL <https://arxiv.org/abs/2405.18392>.

Adam Ibrahim, Benjamin Thérien, Kshitij Gupta, Mats L. Richter, Quentin Anthony, Timothée Lesort, Eugene Belilovsky, and Irina Rish. Simple and scalable strategies to continually pre-train large language models, 2024.

Yiding Jiang, Behnam Neyshabur, Hossein Mobahi, Dilip Krishnan, and Samy Bengio. Fantastic generalization measures and where to find them, 2019.

Tosio Kato. *Perturbation Theory for Linear Operators*. Classics in Mathematics. Springer, Berlin, Heidelberg, 2nd edition, 1995.

Lingkai Kong and Molei Tao. Stochasticity of deterministic gradient descent: Large learning rate for multiscale objective function, 2020.

Timothée Lesort, Oleksiy Ostapenko, Diganta Misra, Md Rifat Arefin, Pau Rodríguez, Laurent Charlin, and Irina Rish. Challenging common assumptions about catastrophic forgetting, 2023.

Yuanzhi Li, Colin Wei, and Tengyu Ma. Towards explaining the regularization effect of initial large learning rate in training neural networks, 2020.

Zhiyuan Li, Sadhika Malladi, and Sanjeev Arora. On the validity of modeling sgd with stochastic differential equations (sdes), 2021.

Zhiyuan Li, Tianhao Wang, and Sanjeev Arora. What happens after sgd reaches zero loss? – a mathematical framework, 2022.

Hong Liu, Sang Michael Xie, Zhiyuan Li, and Tengyu Ma. Same pre-training loss, better downstream: Implicit bias matters for language models, 2022.

Hong Liu, Zhiyuan Li, David Hall, Percy Liang, and Tengyu Ma. Sophia: A scalable stochastic second-order optimizer for language model pre-training, 2024.

Ilya Loshchilov and Frank Hutter. Sgdr: Stochastic gradient descent with warm restarts, 2017.

Kaifeng Lyu, Zhiyuan Li, and Sanjeev Arora. Understanding the generalization benefit of normalization layers: Sharpness reduction, 2023.

Chao Ma, Daniel Kunin, Lei Wu, and Lexing Ying. Beyond the quadratic approximation: the multiscale structure of neural network loss landscapes, 2022.

Sadhika Malladi, Kaifeng Lyu, Abhishek Panigrahi, and Sanjeev Arora. On the sdes and scaling rules for adaptive gradient algorithms, 2023.

Sanket Vaibhav Mehta, Darshan Patil, Sarath Chandar, and Emma Strubell. An empirical investigation of the role of pre-training in lifelong learning, 2023.

Preetum Nakkiran, Gal Kaplun, Dimitris Kalimeris, Tristan Yang, Benjamin L. Edelman, Fred Zhang, and Boaz Barak. Sgd on neural networks learns functions of increasing complexity, 2019.

Matteo Pagliardini, Pierre Ablin, and David Grangier. The ademamix optimizer: Better, faster, older, 2024. URL <https://arxiv.org/abs/2409.03137>.

Yan Pan and Yuanzhi Li. Toward understanding why adam converges faster than sgd for transformers, 2023.

Bowen Peng, Jeffrey Quesnelle, Honglu Fan, and Enrico Shippe. Yarn: Efficient context window extension of large language models, 2023. URL <https://arxiv.org/abs/2309.00071>.

Jack W. Rae, Sebastian Borgeaud, Trevor Cai, Katie Millican, Jordan Hoffmann, Francis Song, John Aslanides, Sarah Henderson, Roman Ring, Susannah Young, Eliza Rutherford, Tom Hennigan, Jacob Menick, Albin Cassirer, Richard Powell, George van den Driessche, Lisa Anne Hendricks, Maribeth Rauh, Po-Sen Huang, Amelia Glaese, Johannes Welbl, Sumanth Dathathri, Saffron Huang, Jonathan Uesato, John Mellor, Irina Higgins, Antonia Creswell, Nat McAleese, Amy Wu, Erich Elsen, Siddhant Jayakumar, Elena Buchatskaya, David Budden, Esme Sutherland, Karen Simonyan, Michela Paganini, Laurent Sifre, Lena Martens, Xiang Lorraine Li, Adhiguna Kuncoro, Aida Nematzadeh, Elena Gribovskaya, Domenic Donato, Angeliki Lazaridou, Arthur Mensch, Jean-Baptiste Lespiau, Maria Tsimpoukelli, Nikolai Grigorev, Doug Fritz, Thibault Sottiaux, Mantas Pajarskas, Toby Pohlen, Zhitao Gong, Daniel Toyama, Cyprien de Masson d’Autume, Yujia Li, Tayfun Terzi, Vladimir Mikulik, Igor Babuschkin, Aidan Clark, Diego de Las Casas, Aurelia Guy, Chris Jones, James Bradbury, Matthew Johnson, Blake Hechtman, Laura Weidinger, Iason Gabriel, William Isaac, Ed Lockhart, Simon Osindero, Laura Rimell, Chris Dyer, Oriol Vinyals, Kareem Ayoub, Jeff Stanway, Lorrayne Bennett, Demis Hassabis, Koray Kavukcuoglu, and Geoffrey Irving. Scaling language models: Methods, analysis & insights from training gopher, 2022.

Colin Raffel, Noam Shazeer, Adam Roberts, Katherine Lee, Sharan Narang, Michael Matena, Yanqi Zhou, Wei Li, and Peter J. Liu. Exploring the limits of transfer learning with a unified text-to-text transformer, 2023.

Elan Rosenfeld and Andrej Risteski. Outliers with opposing signals have an outsized effect on neural network optimization, 2023.

Baptiste Rozière, Jonas Gehring, Fabian Gloeckle, Sten Sootla, Itai Gat, Xiaoqing Ellen Tan, Yossi Adi, Jingyu Liu, Romain Sauvestre, Tal Remez, Jérémie Rapin, Artyom Kozhevnikov, Ivan Evtimov, Joanna Bitton, Manish Bhatt, Cristian Canton Ferrer, Aaron Grattafiori, Wenhan Xiong, Alexandre Défossez, Jade Copet, Faisal Azhar, Hugo Touvron, Louis Martin, Nicolas Usunier, Thomas Scialom, and Gabriel Synnaeve. Code llama: Open foundation models for code, 2024. URL <https://arxiv.org/abs/2308.12950>.

Sunny Sanyal, Atula Neerkaje, Jean Kaddour, Abhishek Kumar, and Sujay Sanghavi. Early weight averaging meets high learning rates for llm pre-training, 2023.

Leslie N. Smith. Cyclical learning rates for training neural networks, 2017.

Samuel L. Smith, Erich Elsen, and Soham De. On the generalization benefit of noise in stochastic gradient descent, 2020.

Minhak Song, Kwangjun Ahn, and Chulhee Yun. Does sgd really happen in tiny subspaces?, 2024. URL <https://arxiv.org/abs/2405.16002>.

Howe Tissue, Venus Wang, and Lu Wang. Scaling law with learning rate annealing, 2024. URL <https://arxiv.org/abs/2408.11029>.

Hugo Touvron, Louis Martin, Kevin Stone, Peter Albert, Amjad Almahairi, Yasmine Babaei, Nikolay Bashlykov, Soumya Batra, Prajjwal Bhargava, Shruti Bhosale, Dan Bikel, Lukas Blecher, Christian Canton Ferrer, Moya Chen, Guillem Cucurull, David Esiobu, Jude Fernandes, Jeremy Fu, Wenyin Fu, Brian Fuller, Cynthia Gao, Vedanuj Goswami, Naman Goyal, Anthony Hartshorn, Saghar Hosseini, Rui Hou, Hakan Inan, Marcin Kardas, Viktor Kerkez, Madian Khabsa, Isabel Kloumann, Artem Korenev, Punit Singh Koura, Marie-Anne Lachaux, Thibaut Lavril, Jenya Lee, Diana Liskovich, Yinghai Lu, Yuning Mao, Xavier Martinet, Todor Mihaylov, Pushkar Mishra, Igor Molybog, Yixin Nie, Andrew Poulton, Jeremy Reizenstein, Rashi Rungta, Kalyan Saladi, Alan Schelten, Ruan Silva, Eric Michael Smith, Ranjan Subramanian, Xiaoqing Ellen Tan, Binh Tang, Ross Taylor, Adina Williams, Jian Xiang Kuan, Puxin Xu, Zheng Yan, Iliyan Zarov, Yuchen Zhang, Angela Fan, Melanie Kambadur, Sharan Narang, Aurelien Rodriguez, Robert Stojnic, Sergey Edunov, and Thomas Scialom. Llama 2: Open foundation and fine-tuned chat models, 2023.

Szymon Tworkowski, Konrad Staniszewski, Mikołaj Pacek, Yuhuai Wu, Henryk Michalewski, and Piotr Miłoś. Focused transformer: Contrastive training for context scaling, 2023.

Tom Veniat, Ludovic Denoyer, and Marc'Aurelio Ranzato. Efficient continual learning with modular networks and task-driven priors, 2021.

Mingze Wang, Jinbo Wang, Haotian He, Zilin Wang, Guanhua Huang, Feiyu Xiong, Zhiyu Li, Weinan E, and Lei Wu. Improving generalization and convergence by enhancing implicit regularization, 2024. URL <https://arxiv.org/abs/2405.20763>.

Yuqing Wang, Minshuo Chen, Tuo Zhao, and Molei Tao. Large learning rate tames homogeneity: Convergence and balancing effect, 2022.

Jingfeng Wu, Peter L. Bartlett, Matus Telgarsky, and Bin Yu. Large stepsize gradient descent for logistic loss: Non-monotonicity of the loss improves optimization efficiency, 2024. URL <https://arxiv.org/abs/2402.15926>.

Kaichao You, Mingsheng Long, Jianmin Wang, and Michael I. Jordan. How does learning rate decay help modern neural networks?, 2019.

Yang You, Jing Li, Sashank Reddi, Jonathan Hseu, Sanjiv Kumar, Srinadh Bhojanapalli, Xiaodan Song, James Demmel, Kurt Keutzer, and Cho-Jui Hsieh. Large batch optimization for deep learning: Training bert in 76 minutes, 2020.

Xiaohua Zhai, Alexander Kolesnikov, Neil Houlsby, and Lucas Beyer. Scaling vision transformers, 2022.

Jingzhao Zhang, Tianxing He, Suvrit Sra, and Ali Jadbabaie. Why gradient clipping accelerates training: A theoretical justification for adaptivity, 2020a.

Jingzhao Zhang, Sai Praneeth Karimireddy, Andreas Veit, Seungyeon Kim, Sashank Reddi, Sanjiv Kumar, and Suvrit Sra. Why are adaptive methods good for attention models? In H. Larochelle, M. Ranzato, R. Hadsell, M.F. Balcan, and H. Lin (eds.), *Advances in Neural Information Processing Systems*, volume 33, pp. 15383–15393. Curran Associates, Inc., 2020b. URL https://proceedings.neurips.cc/paper_files/paper/2020/file/b05b57f6add810d3b7490866d74c0053-Paper.pdf.

A OMITTED PROOFS

A.1 NOTATION.

To denote $a^T b$ for two vectors, we will $\langle a, b \rangle$. We will use the following function to denote the directional derivative of a mapping $F : \mathbb{R}^d \rightarrow \mathbb{R}^m$:

$$\nabla F(x)[v] = \lim_{\alpha \rightarrow 0} \frac{F(x + \alpha v) - F(x)}{\alpha}.$$

A.2 A WARMUP ON THE QUADRATIC FUNCTION

We will first motivate the decaying function we choose Equation (8) using a simple example on quadratic function.

Lemma A.1. *Assuming that we are considering the following gradient descent*

$$y_{k+1} = y_k - \eta_k \nabla(\gamma y_k^2/2) - \eta g_k, g_k \in \mathcal{N}(0, \sigma^2 \mathcal{I}).$$

Suppose $\eta_0 = \eta_{\max}$ and y_0 follows a normal distribution $\mathcal{N}(0, \eta_{\max} \frac{\sigma^2}{2\gamma - \eta_{\max}\gamma^2})$. Then the following two statements hold,

1. *If $\forall t, \eta_t = \eta_0$, y_k will follow the same distribution as y_0 .*
2. *Consider all the learning rate schedule η_k , the following is the optimal*

$$\forall t \geq 1, \eta_k^* = \frac{1}{\gamma(k-1) + \frac{2}{\eta_{\max}}}$$

in the sense that it yields the fastest expected loss decrease. Suppose η_k^ corresponds to iterates variables y_k^* for any η_k and its corresponding iterates variables y_k ,*

$$\mathbb{E}[\gamma y_k^2/2] \geq \mathbb{E}[\gamma(y_k^*)^2/2] = \frac{\sigma^2}{\gamma} \eta_k^*.$$

Proof. We will denote $\sigma_k = \mathbb{E}[y_k^2]$ and assume WLOG we start decaying at step 0. Then we will have

$$\sigma_k = (1 - \eta_k \gamma)^2 \sigma_{k-1} + \eta_k^2 \sigma^2.$$

If we choose all $\eta_k = \eta_{\max}$, we can directly verify that $\sigma_k = \sigma$.

If we choose $\eta_k = \frac{\sigma_{k-1}\gamma}{\sigma_{k-1}\gamma^2 + \sigma^2}$ to minimize the right hand side, we will have that

$$\begin{aligned} \sigma_k &= \frac{\sigma_{k-1}\sigma^2}{\sigma_{k-1}\gamma^2 + \sigma^2}. \\ \iff \frac{1}{\sigma_k} &= \frac{1}{\sigma_{k-1}} + \frac{\gamma^2}{\sigma^2} = \frac{1}{\sigma_0} + \frac{\gamma^2 k}{\sigma^2}. \end{aligned}$$

This implies $\sigma_k = \frac{1}{\frac{1}{\sigma_0} + \frac{\gamma^2 k}{\sigma^2}}$ and plugging into $\eta_k = \frac{\sigma_{k-1}\gamma}{\sigma_{k-1}\gamma^2 + \sigma^2}$ we have that

$$\eta_k^* = \frac{\gamma}{\gamma^2 + \frac{\sigma^2}{\sigma_{k-1}}} = \frac{\gamma}{\gamma^2 k + \frac{\sigma^2}{\sigma_0}} = \frac{\gamma}{\sigma^2} \sigma_k.$$

The optimality of η_k^* can be easily inferred from the proof. \square

A.3 LANDSCAPE ANALYSIS

We will parameterize $P_F(x)$ as $v_d(x)v_d(x)^T$ and $P_S(x)$ to denote $\mathcal{I} - P_F(x)$. Throughout this section, we will assume $v_d(x)$ is continuous and pointing towards the direction of the gradient for all the x on the river. The following technical lemmas will be used repetitively in the proof.

Lemma A.2. *Under Assumptions 1 and 2, the directional derivative of $P_S(x)$ and $P_F(x)$ exist and satisfied that*

$$\nabla P_F(x)[v] = -\nabla P_S(x)[v] = \nabla v_d(x)[v]v_d(x)^T + v_d(x)\nabla v_d(x)[v]^T.$$

Further

$$\nabla P_S(x)[v]P_S a = \langle \nabla v_d(x)[v], P_S a \rangle v_d(x),$$

$$\nabla P_S(x)[v]P_F a = \langle v_d, P_F a \rangle \nabla v_d(x)[v].$$

$$\|\nabla P_S(x)[v]\|_2 \leq \frac{\gamma\epsilon}{\Delta} \|v\|_2.$$

Proof. As γ_{flat} is an unique eigenvalue of $\nabla^2 L(x + vt)$ and $\nabla^2 L(x + vt)$ is analytical with respect to t , by Theorem 6.1 of Kato (1995), we know that $v_d(x + vt)$ is analytical with respect to t . Hence, the directional derivative exists.

The proof is by applying the chain rule and noticing that $\langle v_d(x), \nabla v_d(x)[v] \rangle = 0$ because $v_d(x)$ is always a unit vector. \square

We will now define the projection of iterate to the river as the progress measure of the optimization dynamics.

Definition A.3. *For U in Assumption 2 and any $w \in U$, we define the following ODE as the projection flow:*

$$\phi(w, 0) = w, d\phi(w, t) = -P_S(w)\nabla L(\phi(w, t)) dt. \quad (9)$$

When $\lim_{t \rightarrow \infty} \phi(w, t)$ is well defined, we will define $\Phi(w) = \lim_{t \rightarrow \infty} \phi(w, t)$ as the projection of w to the river.

The following lemma ensures that the projection function is well-defined and is close to w :

Lemma A.4. *Under Assumptions 1 and 2, for any w satisfying that $\mathcal{B}(w, \frac{2\Delta}{\gamma}) \subset U$, $\Phi(w) \in \mathcal{M}$ exists and $\|w - \Phi(w)\|_2 \leq \frac{2\|P_S(w)\nabla L(w)\|_2}{\gamma + 2\gamma_{\text{flat}}}$. Moreover, movement along the projection flow decays exponentially, $\|P_S(\phi(w, t))\nabla L(\phi(w, t))\|_2 \leq \exp(-\gamma t/2)\|P_S(w)\nabla L(w)\|_2$.*

Proof. We will track $\|P_S(\phi(w, t))\nabla L(\phi(w, t))\|_2^2$ along the projection flow before $\phi(w, t)$ leaves U ,

$$\begin{aligned} & \frac{d\|P_S(\phi(w, t))\nabla L(\phi(w, t))\|_2^2}{dt} \\ &= 2\langle P_S(\phi(w, t))\nabla L(\phi(w, t)), \frac{dP_S(\phi(w, t))}{dt}\nabla L(\phi(w, t)) + P_S(\phi(w, t))\frac{d\nabla L(\phi(w, t))}{dt} \rangle. \end{aligned}$$

By Lemma A.2 and assumption 2, the first term can be bounded as

$$\begin{aligned} & \langle P_S(\phi(w, t))\nabla L(\phi(w, t)), \frac{dP_S(\phi(w, t))}{dt}\nabla L(\phi(w, t)) \rangle \\ &= -\langle P_S(\phi(w, t))\nabla L(\phi(w, t)), \nabla P_S(\phi(w, t))[P_S(\phi(w, t))\nabla L(\phi(w, t))]\nabla L(\phi(w, t)) \rangle \\ &= -\langle P_S(\phi(w, t))\nabla L(\phi(w, t)), \nabla v_d(x)[P_S(\phi(w, t))\nabla L(\phi(w, t))]\rangle \langle v_d, P_F(\phi(w, t))\nabla L(\phi(w, t)) \rangle \\ &\leq \|\nabla L(\phi(w, t))\| \|P_S(\phi(w, t))\nabla L(\phi(w, t))\|^2 \frac{\kappa\gamma}{\Delta} \leq \kappa\gamma \|P_S(\phi(w, t))\nabla L(\phi(w, t))\|^2. \end{aligned}$$

The second term is always negative

$$\begin{aligned} & \langle P_S(\phi(w, t))\nabla L(\phi(w, t)), P_S(\phi(w, t))\frac{d\nabla L(\phi(w, t))}{dt} \rangle \\ &= -\langle P_S(\phi(w, t))\nabla L(\phi(w, t)), P_S(\phi(w, t))\nabla^2 L(\phi(w, t))P_S(\phi(w, t))\nabla L(\phi(w, t)) \rangle \\ &\leq -(\gamma + 4\gamma_{\text{flat}})\|P_S(\phi(w, t))\nabla L(\phi(w, t))\|^2. \end{aligned}$$

Summing up the two terms,

$$\frac{d\|P_S(\phi(w, t))\nabla L(\phi(w, t))\|_2^2}{dt} \leq -(\gamma + 2\gamma_{\text{flat}})\|P_S(\phi(w, t))\nabla L(\phi(w, t))\|^2.$$

By Lemma A.34, we have $\|P_S(\phi(w, t))\nabla L(\phi(w, t))\|_2^2 \leq \exp(-(\gamma + 2\gamma_{\text{flat}})t)\|P_S(w)\nabla L(w)\|_2^2$. Hence $\forall t > 0$,

$$\begin{aligned}\|\phi(w, t) - w\|_2 &\leq \int_0^\infty \|P_S(\phi(w, \tau))\nabla L(\phi(w, \tau))\|_2 d\tau \\ &\leq \|P_S(w)\nabla L(w)\|_2 \int_0^\infty \exp(-(\gamma + 2\gamma_{\text{flat}})t/2) \\ &\leq \frac{2\|P_S(w)\nabla L(w)\|_2}{(\gamma + 2\gamma_{\text{flat}})}.\end{aligned}$$

As $\mathcal{B}(w, \frac{\Delta}{2\gamma}) \subset U$, the analysis hold along the trajectory and this shows that $\Phi(w) = \lim_{t \rightarrow \infty} \phi(w, t)$ exists and that $\|\Phi(w) - w\|_2 \leq \frac{2\|P_S(w)\nabla L(w)\|_2}{(\gamma + 2\gamma_{\text{flat}})}$.

Further $\Phi(w)$ satisfies that $P_S(\Phi(w))\nabla L(\Phi(w)) = 0$, and by Assumption 2, $\Phi(w) \in \mathcal{M}$. \square

The following lemmas focus on the properties of $\partial\Phi$.

Lemma A.5. *Under Assumptions 1 and 2, for any w satisfying that $\mathcal{B}(w, \frac{2\Delta}{\gamma}) \subset U$, $\partial\Phi(w)$ is well-defined.*

Proof. Recall that $\Phi(w) = \underbrace{(\phi \circ \phi \circ \dots \circ \phi)}_{n \text{ times}}(w)$, as ϕ is differentiable (Lemma A.2) and \mathcal{M} is the fixed point of Φ , by Theorem 5.1 of Falconer (1983), we have that $\partial\Phi(w)$ is well-defined. \square

Lemma A.6. *Under Assumptions 1 and 2, for any w satisfying that $\mathcal{B}(w, \frac{2\Delta}{\gamma}) \subset U$, it holds that $\partial\Phi(w)P_S(w)\nabla L(w) = 0$. Further for any $w = x(t) \in \mathcal{M}$, it holds that $\partial\Phi(w)P_S(w) = 0$, $\partial\Phi(w)\frac{dx(t)}{dt} = \frac{dx(t)}{dt}$ and that for any v , $\partial\Phi(w)v$ aligns with $\frac{dx(t)}{dt}$.*

Proof. According to Lemmas A.4 and A.6, $\Phi, \partial\Phi$ is well-defined when $\mathcal{B}(w, \frac{2\Delta}{\gamma}) \subset U$. Based on Definition A.3, we have that

$$\forall t, \Phi(\phi(w, t)) = \Phi(w).$$

Hence,

$$\frac{d\Phi(\phi(w, t))}{dt} \Big|_{t=0} = 0,$$

Therefore,

$$0 = \partial\Phi(w) \frac{d\phi(w, t)}{dt} \Big|_{t=0} = -\partial\Phi(w)P_S(w)\nabla L(w).$$

For any $w \in \mathcal{M}$ and any $v \in \mathbb{R}^d$, it holds that

$$\begin{aligned}0 &= \frac{d\partial\Phi(w + \alpha v)P_S(w + \alpha v)\nabla L(w + \alpha v)}{d\alpha} \Big|_{\alpha=0} \\ &= \partial^2\Phi(w)[v]P_S(w)\nabla L(w) + \partial\Phi(w)\left[\partial P_S(w)[v]\nabla L(w) + P_S(w)\nabla^2 L(w)v\right] \\ &= \partial\Phi(w)\left[\partial P_S(w)[v]\nabla L(w) + P_S(w)\nabla^2 L(w)v\right].\end{aligned}\tag{10}$$

Define $J_w(v)$ as the projection from v to $\partial P_S(w)[v]\nabla L(w) + P_S(w)\nabla^2 L(w)v$.

Lemma A.7. *$J_w(v)$ is a linear projection and the range of J_w is the range of P_S .*

Proof. Based on Lemma A.2, $P_S\partial P_S(w)[v]\nabla L(w) = \partial P_S(w)[v]\nabla L(w)$. Hence the range of J_w is a subspace of the range of P_S . When $v = P_S(w)u \neq 0$, based on Assumption 2,

$$\|J_w(v)\|_2 \geq \|P_S\nabla^2 L(w)P_S(w)u\|_2 - \|\partial P_S(w)[P_S(w)u]\nabla L(w)\|_2 \geq \gamma\|u\|_2 - \gamma\kappa\|u\|_2 > 0.$$

Hence the range of J_w has a dimension no smaller than the dimension of the range of $P_S(w)$. This concludes that the range of J_w is the range of $P_S(w)$. \square

Hence by Equation (10) and lemma A.7, it holds that for $w \in \mathcal{M}$, $\partial\Phi(w)P_S(w) = 0$. This shows that the range of $\partial\Phi(w)$ has dimension 1.

Finally for any $w \in \mathcal{M}$, $\Phi(w) = w$. Hence,

$$\begin{aligned} \frac{d\Phi(x(t)) - dx(t)}{dt} &= 0, \\ \partial\Phi(x(t)) \frac{dx(t)}{dt} &= \frac{dx(t)}{dt}. \end{aligned}$$

Hence the range of $\partial\Phi(w)$ contains $\frac{dx(t)}{dt}$, this concludes the proof. \square

Lemma A.8. *Under Assumptions 1 and 2, for any w satisfying that $\mathcal{B}(w, \frac{2\Delta}{\gamma}) \subset U$, it holds that*

$$\begin{aligned} \frac{\|P_F[\Phi(w)]\partial\Phi(w)\nabla L(w) - P_F(w)\nabla L(w)\|_2}{\|P_F(w)\nabla L(w)\|_2} &\leq 5\kappa, \\ \frac{\|P_S[\Phi(w)]\partial\Phi(w)\nabla L(w)\|_2}{\|P_F(w)\nabla L(w)\|_2} &\leq 5\kappa. \end{aligned}$$

Proof. First, by Lemma A.6, it holds that $\partial\Phi(w)\nabla L(w) = \partial\Phi(w)P_F(w)\nabla L(w)$. Define

$$\begin{aligned} v &= P_F(w)\nabla L(w)/\|P_F(w)\nabla L(w)\|_2, \\ s(t) &= P_S(\phi(w, t))\partial\phi(w, t)[v], \\ f(t) &= P_F(\phi(w, t))\partial\phi(w, t)[v], \end{aligned}$$

it holds that $s(0) = 0$ and $f(0) = v$ as $\phi(w, 0) = w$.

We will bound the changes of $s(t)$ and $f(t)$. We will begin with calculating the time derivative of $\partial\phi(w, t)[v]$.

$$\begin{aligned} \frac{d\partial\phi(w, t)[v]}{dt} &= \partial\left(\frac{d\phi(w, t)}{dt}\right)[v] \\ &= -\partial(P_S(\phi(w, t))\nabla L(\phi(w, t)))[v] \\ &= -\partial P_S(\phi(w, t))[\partial\phi(w, t)[v]]\nabla L(\phi(w, t)) \\ &\quad - P_S(\phi(w, t))\nabla^2 L(\phi(w, t))\partial\phi(w, t)[v] \\ &= -\partial P_S(\phi(w, t))[\partial\phi(w, t)[v]]\nabla L(\phi(w, t)) \\ &\quad - P_S(\phi(w, t))\nabla^2 L(\phi(w, t))s(t). \end{aligned} \tag{11}$$

We will now bound $\frac{d\|s(t)\|_2}{dt}$,

$$\begin{aligned} \frac{d\|s(t)\|_2^2}{dt} &= 2\langle s(t), \frac{ds(t)}{dt} \rangle \\ &= 2\langle s(t), \nabla P_S(\phi(w, t))\left[\frac{d\phi(w, t)}{dt}\right]\partial\phi(w, t)[v] + P_S(\phi(w, t))\frac{d\partial\phi(w, t)[v]}{dt} \rangle \\ &= -2\langle s(t), \nabla P_S(\phi(w, t))[P_S(\phi(w, t))\nabla L(\phi(w, t))]\partial\phi(w, t)[v] \rangle \\ &\quad - 2\langle s(t), P_S(\phi(w, t))\frac{d\partial\phi(w, t)[v]}{dt} \rangle. \end{aligned}$$

By Lemmas A.2 and A.4 and assumption 2, the first term satisfies that,

$$\langle s(t), \nabla P_S(\phi(w, t))[P_S(\phi(w, t))\nabla L(\phi(w, t))]\partial\phi(w, t)[v] \rangle \leq \gamma\kappa\|s(t)\|_2\|s(t) + f(t)\|_2.$$

By Equation (11) and assumption 2, the second term satisfies that,

$$\begin{aligned} &\langle s(t), P_S(\phi(w, t))\frac{d\partial\phi(w, t)[v]}{dt} \rangle \\ &= -\langle s(t), \partial P_S(\phi(w, t))[\partial\phi(w, t)[v]]\nabla L(\phi(w, t)) \rangle \\ &\quad - \langle s(t), P_S(\phi(w, t))\nabla^2 L(\phi(w, t))s(t) \rangle \\ &\leq \gamma\kappa\|s(t)\|_2\|s(t) + f(t)\|_2 - \gamma\|s(t)\|_2^2. \end{aligned}$$

Hence $2\|s(t)\|_2 \frac{d\|s(t)\|_2}{dt} = \frac{d\|s(t)\|_2^2}{dt} \leq -2\gamma\|s(t)\|_2^2 + 4\gamma\kappa\|s(t)\|_2\|s(t) + f(t)\|_2$ and we can conclude that

$$\frac{d\|s(t)\|_2}{dt} \leq -\gamma\|s(t)\|_2/2 + 2\gamma\kappa\|f(t)\|_2. \quad (12)$$

Similarly, we can provide a bound for $\|\frac{df(t)}{dt}\|_2$,

$$\begin{aligned} \left\| \frac{df(t)}{dt} \right\| &= 2\|\nabla P_F(\phi(w, t))\left[\frac{d\phi(w, t)}{dt}\right]\partial\phi(w, t)[v] + P_F(\phi(w, t))\frac{d\partial\phi(w, t)[v]}{dt}\|_2 \\ &= -2\|\nabla P_F(\phi(w, t))[P_S(\phi(w, t))\nabla L(\phi(w, t))]\partial\phi(w, t)[v] \\ &\quad + P_F(\phi(w, t))\frac{d\partial\phi(w, t)[v]}{dt}\|_2. \end{aligned}$$

By Lemmas A.2 and A.4 and assumption 2, the first term satisfies that,

$$\begin{aligned} &\|\nabla P_F(\phi(w, t))[P_S(\phi(w, t))\nabla L(\phi(w, t))]\partial\phi(w, t)[v]\| \\ &= \|\nabla P_S(\phi(w, t))[P_S(\phi(w, t))\nabla L(\phi(w, t))]\partial\phi(w, t)[v]\| \\ &\leq \gamma\kappa \exp(-\gamma t/2)\|f(t)\|_2\|s(t) + f(t)\|_2. \end{aligned}$$

By Lemmas A.2 and A.4 and assumption 2, the second term satisfies that,

$$\begin{aligned} &\|P_F(\phi(w, t))\frac{d\partial\phi(w, t)[v]}{dt}\| \\ &= \|P_F(\phi(w, t))\partial P_F(\phi(w, t))[\partial\phi(w, t)[v]]\nabla L(\phi(w, t))\| \\ &= \|P_F(\phi(w, t))\partial P_F(\phi(w, t))[\partial\phi(w, t)[v]]P_S(\phi(w, t))\nabla L(\phi(w, t))\| \\ &\leq \gamma\kappa \exp(-\gamma t/2)\|f(t)\|_2\|s(t) + f(t)\|_2. \end{aligned}$$

Hence we can conclude that

$$\left\| \frac{df(t)}{dt} \right\|_2 \leq 2\gamma\kappa \exp(-\gamma t/2)(\|f(t)\|_2 + \|s(t)\|_2). \quad (13)$$

By Equation (12), it holds that

$$\frac{d(\exp(\gamma t/2)\|s(t)\|_2)}{dt} = \gamma \exp(\gamma t/2)\|s(t)\|_2/2 + \exp(\gamma t/2)\frac{d\|s(t)\|_2}{dt} \leq 2\gamma\kappa \exp(\gamma t/2)\|f(t)\|_2.$$

Integrating the above equation from 0 to t , and we have

$$\|s(t)\|_2 \leq 2\gamma\kappa \int_0^t \exp(\gamma(\tau - t)/2)\|f(\tau)\|_2 d\tau. \quad (14)$$

By Equations (13) and (14), we have that

$$\left| \frac{d\|f(t)\|_2}{dt} \right| \leq 2\gamma\kappa \exp(-\gamma t/2)\|f(t)\|_2 + 4\gamma^2\kappa^2 \int_0^t \exp(\gamma(\tau - 2t)/2)f(\tau)d\tau.$$

This suggests that

$$\|f(T)\|_2 \leq 1 + 2\gamma\kappa \int_0^T \exp(-\gamma t/2)\|f(t)\|_2 dt + 4\gamma^2\kappa^2 \int_0^T \int_0^t \exp(\gamma(\tau - 2t)/2)f(\tau)d\tau dt.$$

Define $M(t) = \sup_{0 \leq \tau \leq t} f(\tau)$, then it holds that

$$\begin{aligned} \|M(T)\|_2 &\leq 1 + \|M(T)\|_2 \left(2\gamma\kappa \int_0^T \exp(-\gamma t/2)dt + 4\gamma^2\kappa^2 \int_0^T \exp(-\gamma t/2) \int_0^t \exp(\gamma(\tau - t)/2)d\tau dt \right) \\ &\leq 1 + \|M(T)\|_2 (4\kappa + 16\kappa^2). \end{aligned}$$

This implies that $\forall t, \|f(t)\|_2 \leq \|M(t)\|_2 \leq \frac{1}{1-4\kappa-16\kappa^2} \leq 1 + 5\kappa$. By Equation (14), this suggests that $\|s(t)\|_2 \leq 4\kappa(1 + 5\kappa) \leq 5\kappa$. Finally, returning to Equation (13), we have that

$$\begin{aligned} \left\| \frac{f(t)}{dt} \right\|_2 &\leq 2\gamma\kappa \exp(-\gamma t/2) (\|f(t)\|_2 + \|s(t)\|_2) \\ &\leq 2\gamma\kappa \exp(-\gamma t/2) (1 + 10\kappa). \end{aligned}$$

Hence $\|f(t) - f(0)\|_2 \leq 2 \int_0^\infty 2\gamma\kappa \exp(-\gamma t/2) (1 + 10\kappa) dt \leq 2\kappa(1 + 10\kappa) \leq 5\kappa$.

We have that

$$\frac{\|P_F[\Phi(w)]\partial\Phi(w)\nabla L(w) - P_F(w)\nabla L(w)\|_2}{\|P_F(w)\nabla L(w)\|_2} = \lim_{t \rightarrow \infty} \|f(t) - f(0)\|_2 \in [0, 5\kappa],$$

and

$$\frac{\|P_S[\Phi(w)]\partial\Phi(w)\nabla L(w)\|_2}{\|P_F(w)\nabla L(w)\|_2} = \lim_{t \rightarrow \infty} \|s(t)\|_2 \in [0, 5\kappa],$$

The proof is then complete. \square

The following lemma generalizes Lemma A.8 to general direction instead of $\nabla L(w)$.

Lemma A.9. *Under Assumptions 1 and 2, for any w satisfying that $\mathcal{B}(w, \frac{2\Delta}{\gamma}) \subset U$, it holds that*

$$\begin{aligned} \frac{\|P_F[\Phi(w)]\partial\Phi(w)u - P_F(w)u\|_2}{\|P_F(w)\nabla L(w)\|_2} &\leq 5\kappa, \\ \frac{\|P_S[\Phi(w)]\partial\Phi(w)u\|_2}{\|P_F(w)u\|_2} &\leq 5\kappa. \end{aligned}$$

Proof. We only need to notice that $P_F(w)u$ aligns with $v_d(\nabla^2 L(w))$. Hence, it always holds that

$$\begin{aligned} P_F(w)u &= P_F(w)\nabla L(w) \frac{\langle P_F(w)\nabla L(w), P_F(w)u \rangle}{\|P_F(w)\nabla L(w)\|_2^2}, \\ \partial\Phi(w)u &= \partial\Phi(w)P_F(w)u = \partial\Phi(w)\nabla L(w) \frac{\langle P_F(w)\nabla L(w), P_F(w)u \rangle}{\|P_F(w)\nabla L(w)\|_2^2}. \end{aligned}$$

The proof is then complete. \square

The following lemma states that the angle between the gradient and the tangent direction is small for any point on the river.

Lemma A.10. *For any $w \in \mathcal{M}$, it holds that*

$$\|P_{\mathcal{M}}(w)\nabla L(w) - \nabla L(w)\|_2 \leq 4\kappa\|P_{\mathcal{M}}(w)\nabla L(w)\|_2.$$

Proof. Assume $w = x(T)$, we will denote $P_{\mathcal{M}}(w)\nabla L(w)$ by v .

It holds that

$$\nabla(P_S(w)\nabla L(w))[v] = 0,$$

which can be simplified to

$$P_S(w)\nabla^2 L(w)v + \nabla P_S(w)[v]\nabla L(w) = 0.$$

The first term satisfies that $\|P_S(w)\nabla^2 L(w)v\|_2 \geq \gamma\|P_S(w)v\|$ and the second term satisfies that $\|\nabla P_S(w)[v]\nabla L(w)\|_2 \leq \gamma\kappa\|v\|$. This then suggests $\|P_S(w)v\|_2 \leq \kappa\|v\|_2$.

Therefore $\|P_F(w)v\|_2 \geq (1 - \kappa)\|v\|_2$. As

$$v = \frac{dx(t)}{dt} \Big|_{t=T} = -P_{\mathcal{M}}(w)\nabla L(w)$$

We know that $|v_d^\top P_{\mathcal{M}}(w)v_d| \geq (1 - \kappa)\|P_{\mathcal{M}}(w)v_d\|_2$, which suggests that $|v_d^\top \frac{P_{\mathcal{M}}(w)v_d}{\|P_{\mathcal{M}}(w)v_d\|_2}| \geq (1 - \kappa)$. Hence we can conclude that $\|P_{\mathcal{M}}(w)v_d\|_2 \geq (1 - \kappa)$. Hence, we know that

$$\|v + \nabla L(w)\|_2 \leq \sqrt{1 - (1 - \kappa)^2} \|\nabla L(w)\|_2 \leq 2\kappa \|\nabla L(w)\|_2 \leq \frac{2\kappa}{1 - \kappa} \|v\|_2 \leq 4\kappa \|v\|_2.$$

This concludes the proof. \square

The next lemma states that $P_F(w)\nabla L(w)$ and $\nabla L(\Phi(w))$ is always close.

Lemma A.11. *Under Assumptions 1 and 2, for any w satisfying that $\mathcal{B}(w, \frac{2\Delta}{\gamma}) \subset U$, it holds that*

$$\|P_F(w)\nabla L(w) - \nabla L(\Phi(w))\|_2 \leq (\gamma\kappa + \gamma_{\text{flat}})\|w - \Phi(w)\|_2.$$

Proof. By Lemma A.4, the line segment from $\Phi(w)$ to w lies in U . By Assumption 2 and lemma A.4,

$$\begin{aligned} & \|P_F(w)\nabla L(w) - P_F(\Phi(w))\nabla L(\Phi(w))\|_2 \\ &= \left\| \int_0^1 \nabla P_F(\Phi(w) + t(w - \Phi(w))) [w - \Phi(w)] \nabla L(\Phi(w) + t(w - \Phi(w))) dt \right. \\ &\quad \left. + \int_0^1 P_F(\Phi(w) + t(w - \Phi(w))) \nabla^2 L(\Phi(w) + t(w - \Phi(w)))(w - \Phi(w)) dt \right\|_2 \\ &\leq (\gamma\kappa + \gamma_{\text{flat}})\|w - \Phi(w)\|_2. \end{aligned}$$

This concludes the proof. \square

The final theorem states that when w is near the river, the movement of its projection has a similar value as the inherent speed at the river.

Lemma A.12. *Under Assumptions 1 and 2, when $\|w - \Phi(w)\|_2 \leq \frac{10\kappa\|P_F(w(t))\nabla L(w(t))\|_2}{\gamma + \gamma_{\text{flat}}}$,*

$$\begin{aligned} & \|P_F(w)\nabla L(w) + \frac{dx(\tau)}{d\tau} \Big|_{\tau=T} \|_2 \leq 16\kappa \left\| \frac{dx(\tau)}{d\tau} \Big|_{\tau=T} \right\|_2, \\ & \|\partial\Phi(w)\nabla L(w) + \frac{dx(\tau)}{d\tau} \Big|_{\tau=T} \|_2 \leq 30\kappa \left\| \frac{dx(\tau)}{d\tau} \Big|_{\tau=T} \right\|_2. \end{aligned}$$

Proof. By Lemma A.8

$$\|\partial\Phi(w)\nabla L(w) - P_F(w)\nabla L(w)\|_2 \leq 10\kappa\|P_F(w)\nabla L(w)\|_2.$$

Combining Lemma A.11 and $\|w - \Phi(w)\|_2 \leq \frac{10\kappa\|P_F(w(t))\nabla L(w(t))\|_2}{\gamma + \gamma_{\text{flat}}}$, we have that

$$\|P_F(w)\nabla L(w) - \nabla L(\Phi(w))\|_2 \leq (\gamma\kappa + \gamma_{\text{flat}})\|w - \Phi(w)\|_2 \leq 10\kappa\|P_F(w)\nabla L(w)\|_2.$$

By Lemma A.10, let $v = \frac{dx(\tau)}{d\tau} \Big|_{\tau=T}$,

$$\|v + \nabla L(\Phi(w))\|_2 \leq 4\kappa\|v\|_2.$$

Combining the three inequalities, we have that

$$\|P_F(w)\nabla L(w) - \nabla L(\Phi(w))\|_2 \leq \frac{10\kappa}{1 - 10\kappa} \|\nabla L(\Phi(w))\|_2 \leq \frac{1 + 4\kappa}{1 - 10\kappa} 10\kappa\|v\|_2 \leq 12\kappa\|v\|_2.$$

This suggests that

$$\|P_F(w)\nabla L(w) - v\|_2 \leq \|P_F(w)\nabla L(w) - \nabla L(\Phi(w))\|_2 + \|v + \nabla L(\Phi(w))\|_2 \leq 16\kappa\|v\|_2.$$

Hence

$$\begin{aligned} & \|v + \partial\Phi(w)\nabla L(w)\|_2 \\ & \leq \|P_F(w)\nabla L(w) - v\|_2 + \|P_F(w)\nabla L(w) - \nabla L(\Phi(w))\|_2 \\ & \leq 16\kappa\|v\|_2 + 10\kappa\|P_F(w)\nabla L(w)\|_2 \\ & \leq 30\kappa\|v\|_2. \end{aligned}$$

This concludes the proof. \square

A.4 PROOF OF THEOREM 3.2

We will consider the following gradient flow:

$$dw(t) = -\nabla L(w(t))dt, w(0) \in V. \quad (15)$$

We will first prove that along the gradient flow trajectory, it holds that $\|P_S(w)\nabla L(w)\|_2$ is bounded.

Lemma A.13. *Under Assumptions 1 and 2, along the gradient flow Equation (15), it holds that for $t \geq 2 \log(2\Delta/(\kappa\Delta_{\min}))/\gamma$, $\|P_S(w(t))\nabla L(w(t))\|_2 \leq 2\kappa\|P_F(w(t))\nabla L(w(t))\|_2$.*

Proof. We will first compute how fast $\|P_S(w(t))\nabla L(w(t))\|_2$ can change

$$\begin{aligned} \frac{d\|P_S(w(t))\nabla L(w(t))\|_2^2}{dt} &= -2\langle P_S(w(t))\nabla L(w(t)), \partial P_S(w(t))[\nabla L(w(t))]\nabla L(w(t)) \rangle \\ &\quad - 2\langle P_S(w(t))\nabla L(w(t)), P_S(w(t))\nabla^2 L(w(t))\nabla L(w(t)) \rangle \end{aligned}$$

By Lemma A.2 and assumption 2, the first term satisfies,

$$\begin{aligned} &-2\langle P_S(w(t))\nabla L(w(t)), \partial P_S(w(t))[\nabla L(w(t))]\nabla L(w(t)) \rangle \\ &= -2\langle P_S(w(t))\nabla L(w(t)), \partial P_S(w(t))[\nabla L(w(t))]\nabla L(w(t)) \rangle \\ &\leq 2\kappa\gamma\|P_S(w(t))\nabla L(w(t))\|_2\|P_F(w(t))\nabla L(w(t))\|_2 \end{aligned}$$

By Assumption 2, the second term satisfies,

$$\begin{aligned} &-2\langle P_S(w(t))\nabla L(w(t)), P_S(w(t))\nabla^2 L(w(t))\nabla L(w(t)) \rangle \\ &\leq -2(\gamma + \gamma_{\text{flat}})\|P_S(w(t))\nabla L(w(t))\|_2^2. \end{aligned}$$

Hence,

$$\frac{d\|P_S(w(t))\nabla L(w(t))\|_2}{dt} \leq \kappa\gamma\|P_F(w(t))\nabla L(w(t))\|_2 - (\gamma + \gamma_{\text{flat}})\|P_S(w(t))\nabla L(w(t))\|_2. \quad (16)$$

We then consider the corresponding $P_F(w(t))\nabla L(w(t))$.

$$\begin{aligned} \frac{d\|P_F(w(t))\nabla L(w(t))\|_2^2}{dt} &= -2\langle P_F(w(t))\nabla L(w(t)), \partial P_F(w(t))[\nabla L(w(t))]\nabla L(w(t)) \rangle \\ &\quad - 2\langle P_F(w(t))\nabla L(w(t)), P_F(w(t))\nabla^2 L(w(t))\nabla L(w(t)) \rangle \end{aligned}$$

By Lemma A.2 and assumption 2, the first term satisfies,

$$\begin{aligned} &-2\langle P_F(w(t))\nabla L(w(t)), \partial P_F(w(t))[\nabla L(w(t))]\nabla L(w(t)) \rangle \\ &= -2\langle P_F(w(t))\nabla L(w(t)), \partial P_F(w(t))[\nabla L(w(t))]\nabla L(w(t)) \rangle \\ &\leq 2\kappa\gamma\|P_S(w(t))\nabla L(w(t))\|_2\|P_S(w(t))\nabla L(w(t))\|_2 \end{aligned}$$

By Assumption 2, the second term satisfies,

$$\begin{aligned} &-2\langle P_F(w(t))\nabla L(w(t)), P_F(w(t))\nabla^2 L(w(t))\nabla L(w(t)) \rangle \\ &\leq 2\gamma_{\text{flat}}\|P_F(w(t))\nabla L(w(t))\|_2^2. \end{aligned}$$

Hence, we have that

$$\left| \frac{d\|P_F(w(t))\nabla L(w(t))\|_2}{dt} \right| \leq \kappa\gamma\|P_S(w(t))\nabla L(w(t))\|_2 + \gamma_{\text{flat}}\|P_F(w(t))\nabla L(w(t))\|_2. \quad (17)$$

Choose $\alpha_\kappa = \frac{1-\sqrt{1-4\kappa^2}}{2\kappa} < 1.5\kappa$ as the solution to the quadratic equation $\kappa\alpha^2 - \alpha + \kappa = 0$.

Then combining Equations (16) and (17), it holds that

$$\begin{aligned} & \frac{d(\|P_S(w(t))\nabla L(w(t))\|_2 - \alpha_\kappa \|P_F(w(t))\nabla L(w(t))\|_2)}{dt} \\ & \leq \gamma(-1 + \kappa\alpha_\kappa) \|P_S(w(t))\nabla L(w(t))\|_2 + \kappa\gamma \|P_F\|_2 \\ & \quad - \gamma_{\text{flat}} (\|P_S(w(t))\nabla L(w(t))\|_2 - \alpha_\kappa \|P_F(w(t))\nabla L(w(t))\|_2). \end{aligned}$$

Notice that

$$\frac{(-1 + \kappa\alpha_\kappa)}{\kappa} = \frac{-1}{\alpha_\kappa}$$

Hence,

$$\begin{aligned} & \frac{d(\|P_S(w(t))\nabla L(w(t))\|_2 - \alpha_\kappa \|P_F(w(t))\nabla L(w(t))\|_2)}{dt} \\ & \leq -(\gamma(1 - \kappa\alpha_\kappa) + \gamma_{\text{flat}}) (\|P_S(w(t))\nabla L(w(t))\|_2 - \alpha_\kappa \|P_F(w(t))\nabla L(w(t))\|_2). \end{aligned}$$

By Lemma A.34, this suggests that

$$\begin{aligned} & \|P_S(w(t))\nabla L(w(t))\|_2 - \alpha_\kappa \|P_F(w(t))\nabla L(w(t))\|_2 \\ & \leq \exp(-(\gamma(1 - \kappa\alpha_\kappa) + \gamma_{\text{flat}})t) (\|P_S(w(0))\nabla L(w(0))\|_2) \\ & \leq \exp(-\gamma t/2) \|P_S(w(0))\nabla L(w(0))\|_2. \end{aligned}$$

Hence,

$$\|P_S(w(t))\nabla L(w(t))\|_2 \leq 1.5\kappa \|P_F(w(t))\nabla L(w(t))\|_2 + \exp(-\gamma t/2) (\|P_S(w(0))\nabla L(w(0))\|_2).$$

□

Lemma A.14. *Under Assumptions 1 and 2, along the gradient flow Equation (15), it holds that $w(t) \in U$ and $\|w(t) - \Phi(w(t))\|_2 \leq \frac{4\kappa \|P_F(w(t))\nabla L(w(t))\|_2 + 2\exp(-\gamma t/2)\Delta}{\gamma + \gamma_{\text{flat}}}$.*

Proof. This is a direct combination of Lemmas A.4 and A.13. □

Lemma A.15. *Under Assumptions 1 and 2, along the gradient flow Equation (15), if $T(t)$ satisfies $x(T(t)) = \Phi(w(t))$, then*

$$\frac{dT(t)}{dt} \in [1 - 30\kappa, 1 + 30\kappa].$$

Proof. As $T(t)$ satisfies $x(T(t)) = \Phi(w(t))$, taking derivative on both sides yield,

$$\frac{dT(t)}{dt} \frac{dx(\tau)}{d\tau} \Big|_{\tau=T(t)} = -\partial\Phi(w(t))\nabla L(w(t)).$$

By Lemmas A.11 and A.14, it holds that

$$\|\partial\Phi(w(t))\nabla L(w(t)) - \frac{dx(\tau)}{d\tau} \Big|_{\tau=T(t)}\|_2 \leq 30\kappa \frac{dx(\tau)}{d\tau} \Big|_{\tau=T(t)}.$$

We then have that

$$\left| \frac{dT(t)}{dt} - 1 \right| \leq 30\kappa,$$

which concludes the proof. □

Proof of Theorem 3.2. The proof is a direct combination of Lemmas A.14 and A.15. □

A.5 PROOF OF THEOREM 3.3

We will consider the following gradient descent:

$$w_{k+1} - w_k = -\eta \nabla L(w_k), w_0 \in \mathcal{M}. \quad (18)$$

We will track the changes of $P_F(w_k) \nabla L(w_k)$ and $P_S(w_k) \nabla L(w_k)$, for simplicity, we will denote them as $fg(k)$ and $sg(k)$. Further, we will use the following denotation

$$w_{k,\tau} = (1 - \tau)w_k + \tau w_{k+1}$$

We will first prove some lemmas bounding the difference between gradient and projections at different points.

Lemma A.16. *Under Assumptions 1 and 2, when $w_k \in V, \forall \tau \in (0, 1), w_{k,\tau} \in U$.*

Proof. It holds that,

$$\|w_k - w_{k,\tau}\|_2 \leq \eta \Delta \leq \frac{\Delta}{2\gamma}.$$

□

Lemma A.17. *Under Assumptions 1 and 2, when $w_k \in V, \forall \tau, \tau' \in [0, 1]$, it holds that*

$$\|P_S(w_{k,\tau}) - P_S(w_{k,\tau'})\|_2 \leq \eta \gamma \kappa.$$

Proof. According to Lemma A.16, it holds that $w_{k,\tau}, w_{k,\tau'} \in U$. Assume without loss of generality $\tau > \tau'$,

$$\begin{aligned} \|P_S(w_{k,\tau}) - P_S(w_{k,\tau'})\| &= \left\| \int_{\tau'}^{\tau} \nabla P_S(w_{k,\tau''}) [\eta \nabla L(w)] d\tau'' \right\|_2 \\ &\leq \int_{\tau'}^{\tau} \|\nabla P_S(w_{k,\tau''}) [\eta \nabla L(w)]\|_2 d\tau'' \\ &\leq \eta \gamma \kappa. \end{aligned}$$

□

Lemma A.18. *Under Assumptions 1 and 2, when $w_k \in V, \forall \tau \in (0, 1)$, it holds that*

$$\|P_S(w_{k,\tau}) \nabla L(w_{k,\tau}) - P_S(w_{k,\tau}) \nabla L(w_k)\|_2 \leq \eta \gamma_{\max} \|sg(k)\|_2 + 2\eta^2 \gamma_{\max} \gamma \kappa \|\nabla L(w_k)\|_2.$$

Proof. According to Lemma A.16, it holds that $w_{k,\tau}, w_{k,\tau'} \in U$. Define $g(\tau') = \|P_S(w_{k,\tau}) \nabla L(w_{k,\tau'}) - P_S(w_{k,\tau}) \nabla L(w_k)\|_2$, then by Lagrange's Mean Value Theorem, there exists τ' , such that

$$\begin{aligned} &\|P_S(w_{k,\tau}) \nabla L(w_{k,\tau}) - P_S(w_{k,\tau}) \nabla L(w_k)\|_2 = g(\tau) - g(0) \\ &= \tau g'(\tau) = \tau \frac{d\|P_S(w_{k,\tau}) \nabla L(w_{k,\tau'}) - P_S(w_{k,\tau}) \nabla L(w_k)\|_2}{d\tau'} \\ &\leq \left\| \frac{dP_S(w_{k,\tau}) \nabla L(w_{k,\tau'}) - dP_S(w_{k,\tau}) \nabla L(w_k)}{d\tau'} \right\|_2 \\ &= \eta \|P_S(w_{k,\tau}) \nabla^2 L(w_{k,\tau'}) \nabla L(w_k)\|_2 \end{aligned}$$

$$\begin{aligned} &\leq \eta \|P_S(w_{k,\tau}) \nabla^2 L(w_{k,\tau'}) P_S(w_{k,\tau'}) \nabla L(w_k)\|_2 + \eta \|P_S(w_{k,\tau}) \nabla^2 L(w_{k,\tau'}) P_F(w_{k,\tau'}) \nabla L(w_k)\|_2 \\ &\leq \eta \gamma_{\max} \|P_S(w_{k,\tau'}) \nabla L(w_k)\|_2 + \eta \|(P_S(w_{k,\tau}) - P_S(w_{k,\tau'})) \nabla^2 L(w_{k,\tau'}) P_F(w_{k,\tau'}) \nabla L(w_k)\|_2. \end{aligned}$$

By Lemma A.17, it holds that

$$\begin{aligned} \gamma_{\max} \|P_S(w_{k,\tau'}) \nabla L(w_k)\|_2 &\leq \gamma_{\max} \|sg(k)\|_2 + \eta \gamma_{\max} \gamma \kappa \|\nabla L(w_k)\|_2. \\ \|(P_S(w_{k,\tau}) - P_S(w_{k,\tau'})) \nabla^2 L(w_{k,\tau'}) P_F(w_{k,\tau'}) \nabla L(w_k)\|_2 &\leq \eta \gamma \gamma_{\text{flat}} \kappa \|\nabla L(w_k)\|_2. \end{aligned}$$

Summing up and the proof is complete. □

Lemma A.19. $\forall \tau \in (0, 1)$, it holds that

$$\|P_S(w_{k,\tau})\nabla L(w_{k,\tau}) - sg(k)\|_2 \leq \|sg(k)\|_2 + 3\eta\gamma\kappa\|\nabla L(w_k)\|_2.$$

Proof. This is a direct combination of Lemmas A.17 and A.18, with

$$\begin{aligned} & \|P_S(w_{k,\tau})\nabla L(w_{k,\tau}) - P_S(w_k)\nabla L(w_k)\|_2 \\ & \leq \|P_S(w_{k,\tau})\nabla L(w_{k,\tau}) - P_S(w_{k,\tau})\nabla L(w_k)\|_2 + \|(P_S(w_{k,\tau}) - P_S(w_k))\nabla L(w_k)\|_2. \end{aligned}$$

The proof is then complete. \square

Lemma A.20. $\forall \tau \in (0, 1)$, it holds that

$$\|P_F(w_{k,\tau})\nabla L(w_{k,\tau}) - P_F(w_{k,\tau})\nabla L(w_k)\|_2 \leq \eta\gamma_{\text{flat}}\|fg(k)\|_2 + 2\eta^2\gamma_{\text{max}}\gamma\kappa\|\nabla L(w_k)\|_2.$$

Proof. Define $g(\tau') = \|P_F(w_{k,\tau})\nabla L(w_{k,\tau'}) - P_F(w_{k,\tau})\nabla L(w_k)\|_2$, then by Lagrange's Mean Value Theorem, there exists τ' , such that

$$\begin{aligned} & \|P_F(w_{k,\tau})\nabla L(w_{k,\tau}) - P_F(w_{k,\tau})\nabla L(w_k)\|_2 = g(\tau) - g(0) \\ & = \tau g'(\tau') = \tau \frac{d\|P_F(w_{k,\tau})\nabla L(w_{k,\tau'}) - P_F(w_{k,\tau})\nabla L(w_k)\|_2}{d\tau'} \\ & \leq \|\frac{dP_F(w_{k,\tau})\nabla L(w_{k,\tau'}) - P_F(w_{k,\tau})\nabla L(w_k)}{d\tau'}\|_2 \\ & = \eta\|P_F(w_{k,\tau})\nabla^2 L(w_{k,\tau'})\nabla L(w_k)\|_2 \\ & \leq \eta\|P_F(w_{k,\tau})\nabla^2 L(w_{k,\tau'})P_F(w_{k,\tau'})\nabla L(w_k)\|_2 + \eta\|P_F(w_{k,\tau})\nabla^2 L(w_{k,\tau'})P_S(w_{k,\tau'})\nabla L(w_k)\|_2 \\ & \leq \eta\gamma_{\text{flat}}\|P_F(w_{k,\tau'})\nabla L(w_k)\|_2 + \eta\|(P_F(w_{k,\tau}) - P_F(w_{k,\tau'}))\nabla^2 L(w_{k,\tau'})P_S(w_{k,\tau'})\nabla L(w_k)\|_2. \end{aligned}$$

By Lemma A.17, it holds that

$$\begin{aligned} & \gamma_{\text{flat}}\|P_F(w_{k,\tau'})\nabla L(w_k)\|_2 \leq \gamma_{\text{flat}}\|fg(k)\|_2 + \eta\gamma_{\text{flat}}\gamma\kappa\|\nabla L(w_k)\|_2. \\ & \|(P_F(w_{k,\tau}) - P_F(w_{k,\tau'}))\nabla^2 L(w_{k,\tau'})P_F(w_{k,\tau'})\nabla L(w_k)\|_2 \leq \eta\gamma\gamma_{\text{max}}\kappa\|\nabla L(w_k)\|_2. \end{aligned}$$

Summing up and the proof is complete. \square

Lemma A.21. $\forall \tau \in (0, 1)$, it holds that

$$\|P_F(w_{k,\tau})\nabla L(w_{k,\tau}) - fg(k)\|_2 \leq \|fg(k)\|_2 + 3\eta\gamma\kappa\|\nabla L(w_k)\|_2.$$

Proof. This is a direct combination of Lemmas A.17 and A.20, with

$$\begin{aligned} & \|P_F(w_{k,\tau})\nabla L(w_{k,\tau}) - P_F(w_k)\nabla L(w_k)\|_2 \\ & \leq \|P_F(w_{k,\tau})\nabla L(w_{k,\tau}) - P_F(w_{k,\tau})\nabla L(w_k)\|_2 + \|(P_F(w_{k,\tau}) - P_F(w_k))\nabla L(w_k)\|_2. \end{aligned}$$

The proof is then complete. \square

We will prove a discrete version of Lemma A.13.

Lemma A.22. Under Assumptions 1 and 2, when $\eta < 1/\gamma_{\text{max}}$, along the gradient flow Equation (18), it holds that $\|P_S(w_k)\nabla L(w_k)\|_2 \leq 10\kappa\|P_F(w_k)\nabla L(w_k)\|_2$ as long as $w(\tau) \in U, \forall \tau \leq k$.

Proof. We will first consider $sg(k)$, By Lagrange's Mean Value Theorem, there exists τ , such that,

$$\begin{aligned} & \|sg(k+1)\|_2^2 - \|sg(k)\|_2^2 \\ & = \|P_S(w_{k,1})\nabla L(w_{k,1})\|_2^2 - \|P_S(w_{k,0})\nabla L(w_{k,0})\|_2^2 = \frac{d\|P_S(w_{k,\tau})\nabla L(w_{k,\tau})\|_2^2}{d\tau} \\ & = -\eta\langle P_S(w_{k,\tau})\nabla L(w_{k,\tau}), \partial P_S(w_{k,\tau})[\nabla L(w_k)]\nabla L(w_{k,\tau}) + P_S(w_{k,\tau})\nabla^2 L(w_{k,\tau})\nabla L(w)\rangle \end{aligned}$$

The first term satisfies that

$$\begin{aligned}
& -\eta \langle P_S(w_{k,\tau}) \nabla L(w_{k,\tau}), \partial P_S(w_{k,\tau}) [\nabla L(w_k)] \nabla L(w_{k,\tau}) \rangle \\
& \leq \eta \gamma \kappa \|\nabla L(w_k)\|_2 \|P_S(w_{k,\tau}) \nabla L(w_{k,\tau})\|_2 \\
& \leq \eta \gamma \kappa \|\nabla L(w_k)\|_2 (2\|sg(k)\|_2 + 3\eta \gamma \kappa \|\nabla L(w_k)\|_2).
\end{aligned}$$

The second term satisfies that

$$\begin{aligned}
& -\eta \langle P_S(w_{k,\tau}) \nabla L(w_{k,\tau}), P_S(w_{k,\tau}) \nabla^2 L(w_{k,\tau}) \nabla L(w_k) \rangle \\
& = -\eta \langle P_S(w_{k,\tau}) \nabla L(w_k), P_S(w_{k,\tau}) \nabla^2 L(w_{k,\tau}) \nabla L(w_k) \rangle + \langle P_S(w_{k,\tau}) (\nabla L(w_k) - \nabla L(w_{k,\tau})), \nabla^2 L(w_{k,\tau}) \nabla L(w_k) \rangle \\
& \leq -\eta (\gamma + 4\gamma_{\text{flat}}) \|P_S(w_{k,\tau}) \nabla L(w_k)\|_2^2 + \eta \gamma_{\max} \|P_S(w_{k,\tau}) \nabla L(w_k)\|_2 \|P_S(w_{k,\tau}) (\nabla L(w_k) - \nabla L(w_{k,\tau}))\|_2
\end{aligned}$$

As we have that $\|a - b\|^2 \geq \frac{\|a\|^2}{2} - 4\|b\|^2$, by Lemma A.17, it holds that

$$\begin{aligned}
& -\|P_S(w_{k,\tau}) \nabla L(w_k)\|_2^2 \\
& = -\|P_S(w_k) \nabla L(w_k) + (P_S(w_{k,\tau}) - P_S(w_k)) \nabla L(w_k)\|_2^2 \\
& \leq -\frac{\|P_S(w_k) \nabla L(w_k)\|_2^2}{2} + 4\|(P_S(w_{k,\tau}) - P_S(w_k)) \nabla L(w_k)\|_2^2 \\
& \leq -\frac{\|P_S(w_k) \nabla L(w_k)\|_2^2}{2} + 4(\eta \gamma \kappa \|\nabla L(w_k)\|)^2. \\
& = -\frac{\|P_S(w_k) \nabla L(w_k)\|_2^2}{2} + 4(\eta \gamma)^2 (\kappa \|\nabla L(w_k)\|)^2. \\
& \leq -\|sg(k)\|_2^2 + 2\eta \gamma \kappa^2 \|\nabla L(w_k)\|^2
\end{aligned}$$

Hence

$$\begin{aligned}
& -\eta (\gamma + 4\gamma_{\text{flat}}) \|P_S(w_{k,\tau}) \nabla L(w_k)\|_2^2 \\
& \leq -\eta (\gamma + 4\gamma_{\text{flat}}) \|sg(k)\|_2^2 + 2\eta^2 (\gamma + 4\gamma_{\text{flat}}) \gamma \kappa^2 \|\nabla L(w_k)\|^2 \\
& \leq -\eta (\gamma + 4\gamma_{\text{flat}}) \|sg(k)\|_2^2 + 2\eta \gamma \kappa^2 \|\nabla L(w_k)\|^2
\end{aligned}$$

By Lemmas A.17 and A.18 and $\eta \gamma_{\max}^2 \leq \gamma/2$, it holds that

$$\begin{aligned}
& \eta \gamma_{\max} \|P_S(w_{k,\tau}) \nabla L(w_k)\|_2 \|P_S(w_{k,\tau}) (\nabla L(w_k) - \nabla L(w_{k,\tau}))\|_2 \\
& \leq \eta^2 \gamma_{\max}^2 (\|sg(k)\|_2 + \eta \gamma \kappa \|\nabla L(w_k)\|_2) (\|sg(k)\|_2 + 2\eta \gamma \kappa \|\nabla L(w_k)\|_2) \\
& \leq \eta \gamma (\|sg(k)\|_2 + \kappa \|\nabla L(w_k)\|_2/2) (\|sg(k)\|_2 + \kappa \|\nabla L(w_k)\|_2)/2.
\end{aligned}$$

Hence, we can conclude that

$$\begin{aligned}
& \|sg(k+1)\|_2^2 - \|sg(k)\|_2^2 \\
& - \eta ((\gamma + 4\gamma_{\text{flat}}) \|sg(k)\|_2^2 + 4\eta \gamma \kappa^2 \|\nabla L(w_k)\|^2) \\
& + \eta \gamma (\|sg(k)\|_2 + \kappa \|\nabla L(w_k)\|_2/2) (\|sg(k)\|_2 + \kappa \|\nabla L(w_k)\|_2)/2
\end{aligned}$$

Let $b = \kappa \|\nabla L(w_k)\|_2$ and $a = sg(k)$, as $b(2a + 3b/2) - a^2 + 4b^2 + \frac{1}{2}(a + b)(a + b) \leq -\frac{a^2}{4} + 10b^2$, it holds that

$$\|sg(k+1)\|_2^2 - \|sg(k)\|_2^2 \leq -\eta \gamma \frac{\|sg(k)\|_2^2}{4} + 10\eta \gamma \kappa^2 \|\nabla L(w_k)\|^2 - 4\eta \gamma_{\text{flat}} \|sg(k)\|_2^2 \quad (19)$$

Similarly, we can control the $fg(k)$ changes. By Lagrange's Mean Value Theorem, there exists τ' , such that,

$$\begin{aligned}
& \|fg(k+1)\|_2^2 - \|fg(k)\|_2^2 \\
& = \|P_F(w_{k,1}) \nabla L(w_{k,1})\|_2^2 - \|P_F(w_{k,0}) \nabla L(w_{k,0})\|_2^2 = \frac{d\|P_F(w_{k,\tau}) \nabla L(w_{k,\tau})\|_2^2}{d\tau} \\
& = -\eta \langle P_F(w_{k,\tau}) \nabla L(w_{k,\tau}), \partial P_F(w_{k,\tau}) [\nabla L(w_k)] \nabla L(w_{k,\tau}) + P_F(w_{k,\tau}) \nabla^2 L(w_{k,\tau}) \nabla L(w) \rangle
\end{aligned}$$

The first term satisfies that

$$\begin{aligned}
& \eta \langle P_F(w_{k,\tau}) \nabla L(w_{k,\tau}), \partial P_F(w_{k,\tau}) [\nabla L(w_k)] \nabla L(w_{k,\tau}) \rangle \\
& \leq \gamma \eta \kappa \|\nabla L(w_k)\|_2 \|P_F(w_{k,\tau}) \nabla L(w_{k,\tau})\|_2 \\
& \leq \gamma \eta \kappa \|\nabla L(w_k)\|_2 (\|fg(k)\|_2 + \eta \gamma_{\text{flat}} \|fg(k)\|_2 + 2\eta^2 \gamma_{\max} \gamma \kappa \|\nabla L(w_k)\|_2) \\
& \leq 4\gamma \eta \kappa \|\nabla L(w_k)\|_2^2.
\end{aligned}$$

Similarly, the second term satisfies that

$$\begin{aligned}
& \eta \langle P_F(w_{k,\tau}) \nabla L(w_{k,\tau}), P_F(w_{k,\tau}) \nabla^2 L(w_{k,\tau}) \nabla L(w) \rangle \\
& \leq \eta \gamma_{\text{flat}} \|P_F(w_{k,\tau}) \nabla L(w_k)\|_2 \|P_F(w_{k,\tau}) \nabla L(w_{k,\tau})\|_2 \\
& \leq \eta \gamma_{\text{flat}} (\|fg(k)\|_2 + \eta \gamma \kappa \|\nabla L(w_k)\|_2) (\|fg(k)\|_2 + \eta \gamma_{\text{flat}} \|fg(k)\|_2 + 2\eta^2 \gamma_{\max} \gamma \kappa \|\nabla L(w_k)\|_2) \\
& \leq 2\eta \gamma_{\text{flat}} (\|fg(k)\|_2 + \eta \gamma \kappa \|\nabla L(w_k)\|_2)^2 \\
& \leq 4\eta \gamma_{\text{flat}} \|fg(k)\|_2^2 + 4\eta^2 \gamma^2 \kappa^2 \|\nabla L(w_k)\|_2^2
\end{aligned}$$

Summarizing and we have

$$\|fg(k+1)\|_2^2 - \|fg(k)\|_2^2 \geq -5\gamma \eta \kappa \|\nabla L(w_k)\|_2^2 - 4\eta \gamma_{\text{flat}} \|fg(k)\|_2^2 \quad (20)$$

Let a_κ be the smaller positive solution of

$$5\kappa a^2 + (10\kappa^2 + 5\kappa - \frac{1}{4})a + 10\kappa^2 = 0.$$

$$\text{Then } a_\kappa = \frac{(-10\kappa^2 - 5\kappa + \frac{1}{4}) - \sqrt{(-10\kappa^2 - 5\kappa + \frac{1}{4})^2 - 200\kappa^3}}{10\kappa} < 100\kappa^2.$$

Then combining Equations (19) and (20)

$$\begin{aligned}
& \|sg(k+1)\|_2^2 - a_\kappa \|fg(k+1)\|_2^2 \\
& \leq (1 - 4\eta \gamma_{\text{flat}}) (\|sg(k)\|_2^2 - a_\kappa \|fg(k+1)\|_2^2) - \eta \gamma (\frac{1}{4} + 10\kappa^2 - 5\kappa a_\kappa) \|sg(k)\|_2^2 + \eta \gamma (10\kappa^2 + 5\kappa a_\kappa) \|fg(k)\|_2^2 \\
& = (1 - 4\eta \gamma_{\text{flat}} - \eta \gamma (\frac{1}{4} + 10\kappa^2 - 5\kappa a_\kappa)) (\|sg(k)\|_2^2 - a_\kappa \|fg(k)\|_2^2).
\end{aligned}$$

As $\|sg(0)\|_2^2 - a_\kappa \|fg(0)\|_2^2 < 0$, we have that $\|sg(k)\|_2^2 < a_\kappa \|fg(k+1)\|_2^2 < 100\kappa^2 \|fg(k)\|_2^2$ for all the t . \square

Then we can show that gradient descent will also track the river closely.

Lemma A.23. *Under Assumptions 1 and 2, along the gradient descent Equation (18), it holds that $w_k \in U$ and $\|w_k - \Phi(w_k)\|_2 \leq \frac{10\kappa \|P_F(w_k) \nabla L(w_k)\|_2}{\gamma + \gamma_{\text{flat}}}$.*

Proof. This is a direct combination of Lemmas A.4 and A.22. \square

Finally, we will show that the movement of the projection of the gradient flow moves approximately at the same rate as the river, a discrete version of Lemma A.14.

Lemma A.24. *Under Assumptions 1 and 2, along the gradient flow Equation (15), along the gradient descent Equation (18), if $T(t)$ satisfies $x(T(t)) = \Phi(w_{[t],t-[t]})$ where $[t]$ is the integer part of t , then for any t that is not integer*

$$\frac{dT(t)}{dt} \in [\eta - (30\kappa + 4\eta \gamma_{\text{flat}})\eta, \eta + (30\kappa + 4\eta \gamma_{\text{flat}})\eta].$$

Proof. Let $[t] = k, t - [t] = \tau$, as $T(t)$ satisfies $x(T(t)) = \Phi(w(k, t - [t]))$, let $v = \frac{dx(\tau)}{d\tau} |_{\tau=T(t)}$, taking derivative on both sides yield,

$$\frac{dT(t)}{dt} v = -\eta \partial \Phi(w_{k,\tau}) \nabla L(w_k).$$

As the proof of Lemma A.20, there exists τ'

$$\begin{aligned} & \|P_F(w_{k,\tau})\nabla L(w_k) - P_F(w_{k,\tau})\nabla L(w_{k,\tau})\|_2 \\ & \leq \eta \|P_F(w_{k,\tau})\nabla^2 L(w_{k,\tau'})P_F(w_{k,\tau'})\nabla L(w_k)\|_2 + \eta \|P_F(w_{k,\tau})\nabla^2 L(w_{k,\tau'})P_S(w_{k,\tau'})\nabla L(w_k)\|_2 \\ & \leq \eta\gamma_{\text{flat}}\|P_F(w_{k,\tau'})\nabla L(w_k)\|_2 + \eta^2\gamma\kappa\gamma_{\text{max}}\|\nabla L(w_k)\|_2 \end{aligned}$$

By Lemma A.17, it holds that

$$\begin{aligned} & \|P_F(w_{k,\tau})\nabla L(w_k) - P_F(w_{k,\tau})\nabla L(w_{k,\tau})\|_2 \\ & \leq \eta\gamma_{\text{flat}}\|P_F(w_{k,\tau})\nabla L(w_k)\|_2 + 2\eta^2\gamma\gamma_{\text{max}}\kappa\|\nabla L(w_k)\|_2 \\ & \leq \eta\gamma_{\text{flat}}\|P_F(w_{k,\tau})\nabla L(w_k)\|_2 + \kappa\|\nabla L(w_k)\|_2 \end{aligned} \quad (21)$$

By Lemma A.22,

$$\begin{aligned} \|\nabla L(w_k)\|_2 & \leq \frac{1}{1-10\kappa}\|P_F(w_k)\nabla L(w_k)\|_2 \\ & \leq \frac{1}{1-10\kappa}(\|P_F(w_{k,\tau})\nabla L(w_k)\|_2 + \eta\gamma\kappa\|\nabla L(w_k)\|_2) \end{aligned}$$

This shows that

$$\|\nabla L(w_k)\|_2 \leq \frac{1}{1-10\kappa-\eta\gamma\kappa}\|P_F(w_{k,\tau})\nabla L(w_k)\|_2 \leq (1+12\kappa)\|P_F(w_{k,\tau})\nabla L(w_k)\|_2$$

Combining with Equation (21), we have that

$$\begin{aligned} & \|P_F(w_{k,\tau})\nabla L(w_k) - P_F(w_{k,\tau})\nabla L(w_{k,\tau})\|_2 \\ & \leq \eta\gamma_{\text{flat}}\|P_F(w_{k,\tau})\nabla L(w_k)\|_2 + \kappa(1+12\kappa)\|P_F(w_{k,\tau})\nabla L(w_k)\|_2 \\ & \leq (\eta\gamma_{\text{flat}} + 2\kappa)\|P_F(w_{k,\tau})\nabla L(w_k)\|_2 \end{aligned}$$

This shows that

$$\begin{aligned} \|P_F(w_{k,\tau})\nabla L(w_k) - P_F(w_{k,\tau})\nabla L(w_{k,\tau})\|_2 & \leq \frac{(\eta\gamma_{\text{flat}} + 2\kappa)}{1-(\eta\gamma_{\text{flat}} + 2\kappa)}\|P_F(w_{k,\tau})\nabla L(w_{k,\tau})\|_2 \\ & \leq (2\eta\gamma_{\text{flat}} + 3\kappa)\|P_F(w_{k,\tau})\nabla L(w_k)\|_2 \end{aligned} \quad (22)$$

By Lemma A.12

$$\|P_F(w_{k,\tau})\nabla L(w_{k,\tau}) + v\|_2 \leq 16\kappa\|v\|_2 \quad (23)$$

Combining Equations (22) and (23),

$$\begin{aligned} & \|P_F(w_{k,\tau})\nabla L(w_k) + v\|_2 \\ & \leq \|P_F(w_{k,\tau})\nabla L(w_k) - P_F(w_{k,\tau})\nabla L(w_{k,\tau})\|_2 + \|P_F(w_{k,\tau})\nabla L(w_{k,\tau}) + v\|_2 \\ & \leq (2\eta\gamma_{\text{flat}} + 3\kappa)\|P_F(w_{k,\tau})\nabla L(w_k)\|_2 + 16\kappa\|v\|_2 \\ & \leq ((2\eta\gamma_{\text{flat}} + 3\kappa)(1+16\kappa) + 16\kappa)\|v\|_2 \\ & \leq (19\kappa + 3\eta\gamma_{\text{flat}})\|v\|_2. \end{aligned} \quad (24)$$

By Lemma A.9

$$\|\partial\Phi(w_{k,\tau})\nabla L(w_k) - P_F(w_{k,\tau})\nabla L(w_k)\|_2 \leq 10\kappa\|P_F(w_{k,\tau})\nabla L(w_k)\|_2. \quad (25)$$

Combining Equations (24) and (25), it holds that

$$\begin{aligned} & \|\partial\Phi(w_{k,\tau})\nabla L(w_k) + v\|_2 \\ & \leq \|\partial\Phi(w_{k,\tau})\nabla L(w_k) - P_F(w_{k,\tau})\nabla L(w_k)\|_2 + \|P_F(w_{k,\tau})\nabla L(w_k) + v\|_2 \\ & \leq 10\kappa\|P_F(w_{k,\tau})\nabla L(w_k)\|_2 + (19\kappa + 3\eta\gamma_{\text{flat}})\|v\|_2 \\ & \leq (30\kappa + 4\eta\gamma_{\text{flat}})\|v\|_2. \end{aligned}$$

Hence

$$\frac{dT(t)}{dt} \in [\eta - (30\kappa + 4\eta\gamma_{\text{flat}})\eta, \eta + (30\kappa + 4\eta\gamma_{\text{flat}})\eta].$$

This concludes the proof. \square

Proof of Theorem 3.3. The proof is a direct combination of Lemmas A.23 and A.24. \square

A.6 PROOF OF THEOREM 3.4

We will first show that under Assumption 3, the loss is separable within U .

Lemma A.25. *Under Assumptions 1 to 3, the river is a straight line parallel to v_d .*

Proof. In this case, the κ in Assumption 2 is 0 and this is a direct corollary of of Lemma A.12. \square

Lemma A.26. *Under Assumptions 1 to 3, there exists functions g and h , such that for any $w \in U$ satisfying that $\mathcal{B}(w, \frac{2\Delta}{\gamma}) \subset U$, it holds that*

$$L(w) = g(\Phi(w)) + h(w - \Phi(w)).$$

Furthermore, h is a γ -strongly convex function when constrained on the range of P_S .

Proof. We will choose g as the constraint of L on \mathcal{M} . Now $w - \Phi(w)$ will always fall in the range of P_S . Consider any y in the range of P_S and as $\nabla v_d(w)[v] = 0$, we have that

$$y^T \nabla^2 L(w) v_d = 0.$$

This then suggest that

$$\nabla[\langle \nabla L(w), y \rangle][v_d] = 0.$$

We then have for any $a \in \mathcal{M}$, by Lemma A.25,

$$\begin{aligned} L(w) - L(\Phi(w)) &= \int_0^1 \langle (w - \Phi(w)), \nabla L(\Phi(w) + \tau(w - \Phi(w))) \rangle d\tau \\ &= \int_0^1 \langle (w - \Phi(w)), \nabla L(a + \tau(w - \Phi(w))) \rangle d\tau. \end{aligned}$$

We will then define $h(w - \Phi(w)) = \int_0^1 \langle (w - \Phi(w)), \nabla L(a + \tau(w - \Phi(w))) \rangle d\tau$. and this concludes the proof.

Now, as $h(w - \Phi(w)) = L(w) - L(\Phi(w))$, $\nabla^2 h(y)$ when constrained on the range of P_S has an eigenvalue greater than γ . \square

We will first consider the mixing dynamics of the current SGD iterates on a strongly convex loss h with a minimizer at 0.

$$y(k+1) = y_k - \eta \nabla h(y_k) - \eta g_k, y(0) = 0, g_k \sim \mathcal{N}(0, \sigma^2 \mathcal{I}) \quad (26)$$

We will define a coupling process \tilde{y}_k as

$$\tilde{y}(k+1) = \tilde{y}_k - \eta H \tilde{y}_k - \eta g_k, w(0) = 0, g_k \sim \mathcal{N}(0, \sigma^2 \mathcal{I}), \tilde{y}(0) = 0. \quad (27)$$

Here $H = \nabla^2 h(0)$ is positive definite.

Assumption 6 (Regularity of h). *We will assume the following for the function h , constant $\delta \in (0, 1]$, learning rate η .*

1. *The smallest eigenvalue of $\nabla^2 h(y)$ within $\mathcal{B}(0, r)$ is at least $\gamma > 0$ and the largest eigenvalue for H is at most γ_{\max} .*
2. $\forall y, h(y) \in [0, M]$.
3. $\forall y \in \mathcal{B}(0, r), \|\nabla h(y)\|_2 \leq \Delta, \|\nabla^3 h(y)\|_2 \leq \rho$.
4. $T > 1/\gamma$.
5. $\eta < 1/(2\gamma_{\max})$.
6. $\eta \rho^2 \sigma^2 \leq \gamma^3 / (1600d \log(8\gamma T/\delta))$.
7. $10 \frac{\sqrt{\eta}\sigma}{\sqrt{\gamma}} \sqrt{d \log(8\gamma T/\delta)} + 400\eta\rho\sigma^2 d \log(8\gamma T/\delta)/\gamma^2 \leq r$.

We will first show that \tilde{y}_k will be bounded with a high probability for T/η steps.

Lemma A.27. *For any $\delta \in (0, 1]$, with probability $1 - \delta$, for \tilde{y}_k defined in Equation (27), under Assumption 6, it holds that for any $k \leq T/\eta$,*

$$\|\tilde{y}_k\|_2 \leq \frac{10\sqrt{\eta}\sigma}{\sqrt{\gamma}} \sqrt{d \log(8\gamma T/\delta)}.$$

Proof. For integer $I = \lceil \gamma T \rceil$. We first have that for $i \leq I$

$$\tilde{y}_{i \lceil \frac{1}{\eta\gamma} \rceil} = (1 - \eta\gamma)^{\lceil \frac{1}{\eta\gamma} \rceil} \tilde{y}_{(i-1) \lceil \frac{1}{\eta\gamma} \rceil} + \eta \sum_{\tau=0}^{\lceil \frac{1}{\eta\gamma} \rceil} (1 - \eta\gamma)^{\lceil \frac{1}{\eta\gamma} \rceil - t} g_{(i-1) \lceil \frac{1}{\eta\gamma} \rceil + \tau}.$$

Denote $\bar{g}_k = \eta \sum_{\tau=0}^{\lceil \frac{1}{\eta\gamma} \rceil} (1 - \eta\gamma)^{\lceil \frac{1}{\eta\gamma} \rceil - t} g_{(i-1) \lceil \frac{1}{\eta\gamma} \rceil + \tau}$, then g_k is a normal vector with variance

$$\eta^2 \sum_{\tau=0}^{\lceil \frac{1}{\eta\gamma} \rceil} (1 - \eta\gamma)^{2(\lceil \frac{1}{\eta\gamma} \rceil - t)} \sigma^2 \mathcal{I} \leq \frac{\eta\sigma^2}{2\gamma - \eta\gamma^2} \leq \frac{\eta\sigma^2}{\gamma}.$$

Further, denote $Y_i = y_{i \lceil \frac{1}{\eta\gamma} \rceil}$ and $e_\gamma = (1 - \eta\gamma)^{\lceil \frac{1}{\eta\gamma} \rceil} < \frac{1}{e}$, then

$$Y_i = e_\gamma Y_{i-1} + \bar{g}_{i-1} = \sum_{j \leq i-1} e_\gamma^{j-1} g_{i-j}$$

Then each variable Y_i is also a Gaussian variable with variance smaller than

$$\sum_{j \leq i-1} e_\gamma^{2(j-1)} \mathbb{E}[\bar{g}_{i-j}^T \bar{g}_{i-j}] \leq \frac{1}{1 - 1/e^2} \frac{\eta\sigma^2}{\gamma} \mathcal{I} \leq \frac{2\eta\sigma^2}{\gamma} \mathcal{I}.$$

Hence, by Lemma A.35, for each i , it holds that

$$\mathbb{P}(\left|Y_i\right| > \frac{2\sqrt{\eta}\sigma}{\sqrt{\gamma}} \sqrt{d \log(4I/\delta)}) < \delta/2I.$$

Using union bound,

$$\mathbb{P}(\exists i \leq I, \left|Y_i\right| > \frac{2\sqrt{\eta}\sigma}{\sqrt{\gamma}} \sqrt{d \log(4I/\delta)}) < \delta/2.$$

We now proceed to bound the distance of y_k compared with close Y_i , without loss of generality, considering $i = 0$, we will define a new process called m_k satisfying that

$$m_k = \sum_{j \leq k} (1 - \eta\gamma)^{\lceil \frac{1}{\eta\gamma} \rceil - j} g_j.$$

Then m_k is a martingale and each m_k is a Gaussian vector. In particular, $m_{\lceil \frac{1}{\eta\gamma} \rceil} = \bar{g}_1$. This further suggests that $\|m_k\|^2$ is a super martingale

$$\mathbb{E}[\|m_k\|_2^2 \mid m_{k-1}] \geq \|m_{k-1}\|_2^2.$$

By Doob's lemma (Lemma A.36)

$$\begin{aligned} \mathbb{P}(\sup_{k \leq \lceil \frac{1}{\eta\gamma} \rceil} \|m_k\|_2^2 > C^2) &\leq \mathbb{P}(\sup_{k \leq \lceil \frac{1}{\eta\gamma} \rceil} \exp(\lambda \|m_k\|_2^2) > \exp(\lambda C^2)) \\ &\leq \mathbb{E}[\exp(\lambda \|m_{\lceil \frac{1}{\eta\gamma} \rceil}\|_2^2 - \lambda C^2)] \\ &= \mathbb{E}[\exp(\lambda \|\bar{g}_1\|_2^2 - \lambda C^2)]. \end{aligned}$$

Following the same line of proof as Lemma A.35, we have that

$$\mathbb{P}\left(\sup_{k \leq \lceil \frac{1}{\eta\gamma} \rceil} \|m_k\|_2 > \frac{2\sqrt{\eta\sigma}}{\sqrt{\gamma}} \sqrt{d \log(4K/\delta)}\right) \leq \delta/2K$$

We further note that $|y_k - Y_0| \leq (1 - \eta\gamma)^{-\lceil \frac{1}{\eta\gamma} \rceil} m_k \leq 4m_k$. We have that for any $k < K$

$$\mathbb{P}\left(\sup_{k \leq \lceil \frac{1}{\eta\gamma} \rceil} \|y_k - Y_0\|_2 > \frac{8\sqrt{\eta\sigma}}{\sqrt{\gamma}} \sqrt{d \log(4K/\delta)}\right) \leq \delta/2K$$

Combining with the bound on Y_k , we have that

$$\mathbb{P}\left(\sup_{0 \leq k \leq T} |y_k| > \frac{10\sqrt{\eta\sigma}}{\sqrt{\gamma}} \sqrt{d \log(8\gamma T/\delta)}\right) \leq \delta.$$

The proof is then complete. \square

The following lemma states that y_k and \tilde{y}_k are close with high probability.

Lemma A.28. *Assume function $h(y)$ is γ -strong convex in $\mathcal{B}(0, r)$ and has a minimizer at 0, then for $\delta \in (0, 1)$, under Assumption 6, it holds that with probability $1 - \delta$,*

$$\forall k < T/\eta, \|\tilde{y}_k - y_k\|_2 \leq 400\eta\rho\sigma^2 d \log(8\gamma T/\delta)/\gamma^2, y_k \in \mathcal{B}(0, r), \tilde{y}_k \in \mathcal{B}(0, r)$$

Proof. By Lemma A.27, with probability $1 - \delta$,

$$\forall k < T/\eta, \|\tilde{y}_k\|_2^2 \leq \frac{100\eta\sigma^2}{\gamma} d \log(8\gamma T/\delta)$$

We will use C as a shorthand for $100d \log(8\gamma T/\delta)$. Under such scenario, define $\nu_k = \tilde{y}_k - y_k$, we will prove by induction for $k \leq T/\eta$ that

$$\|\nu_k\|_2 \leq 4\eta\rho\sigma^2 C/\gamma^2, y_k \in \mathcal{B}(0, r). \quad (28)$$

Clearly $\nu_0 = 0$, satisfies the induction hypothesis. Assuming Equation (28) hold for t , then

$$\begin{aligned} y(k+1) &= y_k - \eta \nabla L(y_k) - \eta g_k \\ &= y_k - \eta \nabla^2 L(0) y_k + e_k - \eta g_k \\ &= \tilde{y}_k (1 - \eta \nabla^2 L(0)) - \eta g_k + \nu_k (1 - \eta \nabla^2 L(0)) + e_k. \end{aligned}$$

Here $\|e_k\| = \|-\eta(\nabla L(y_k) - \eta \nabla^2 L(0)y_k)\|_2 \leq \eta\rho\|y_k\|_2^2 \leq 2\eta\rho(\|\tilde{y}_k\|_2^2 + \|\nu_k\|_2^2)$. Hence we have that

$$\|\nu_{k+1}\|_2 \leq (1 - \eta\gamma)\|\nu_k\|_2 + 2\eta\rho(\|\tilde{y}_k\|_2^2 + \|\nu_k\|_2^2).$$

As $\|\nu_k\| \leq 4\frac{\eta\rho\sigma^2 C}{\gamma^2} \leq \frac{\gamma}{4\rho}$, we have that $2\rho\|\nu_k\|_2^2 \leq \eta\gamma\|\nu_k\|_2^2/2$.

Hence

$$\begin{aligned} \|\nu_{k+1}\|_2 &\leq (1 - \eta\gamma/2)\|\nu_k\|_2 + 2\eta\rho\frac{\eta\sigma^2 C}{\gamma} \\ &= (1 - \eta\gamma/2)\|\nu_k\|_2 + 2\frac{\eta^2\rho\sigma^2 C}{\gamma} \end{aligned}$$

By induction $\|\nu_k\|_2 \leq 4\eta\rho\sigma^2 C/\gamma^2$. It is then easy to check $\|\nu_{k+1}\|_2 \leq 4\eta\rho\sigma^2 C/\gamma^2$. \square

The following lemma tracks the changes of $\mathbb{E}[h(y_k)]$.

Lemma A.29. Assume function $h(y)$ is γ -strong convex in $\mathcal{B}(0, r)$ and has a minimizer at 0, then for $\delta \in (0, 1)$, denote $100 \log(8\gamma T/\delta)$ as C , under Assumption 6, it holds that $\forall t \in [1/\eta\gamma, T/\eta]$,

$$\left| \mathbb{E}[h(\tilde{y}_k)] - \eta\sigma^2 d/2 \right| \leq \eta^2\sigma^2 \text{Tr}(H) + \frac{\Delta\rho C}{\gamma^2} d\eta\sigma^2 + \rho \left(\frac{d\eta\sigma^2 C}{\gamma} \right)^{3/2} + 2\delta M + \delta\eta\sigma^2 d/2$$

Proof. By Lemma A.28, with probability $1 - \delta$,

$$\|\tilde{y}_k - y_k\|_2 \leq 4\eta\rho d\sigma^2 C/\gamma^2, y_k \in \mathcal{B}(0, r), \tilde{y}_k \in \mathcal{B}(0, r).$$

Define this event as \mathcal{E}_1 .

Hence

$$\begin{aligned} & \left| \mathbb{E}[h(y_k)] - \mathbb{E}[h(\tilde{y}_k)] \right| \\ & \leq \left| \mathbb{E}[h(\tilde{y}_k) - h(y_k) \mid \mathcal{E}_1] \mathbb{P}(\mathcal{E}_1) + \mathbb{E}[h(\tilde{y}_k) - h(y_k) \mid \mathcal{E}_1^c] \mathbb{P}(\mathcal{E}_1^c) \right| \\ & \leq 4 \frac{\Delta\rho C}{\gamma^2} \eta d\sigma^2 + \delta M. \end{aligned}$$

For $\|y\|_2 < r$, it holds that

$$\|h(y) - y^T \nabla^2 h(0) y\|_2 \leq \rho \|y\|_2^3.$$

By Lemma A.27, with probability $1 - \delta$, for $\eta < 1/\gamma_{\max}$, it holds that for any $k \leq T/\eta$,

$$\|\tilde{y}_k\|_2^2 \leq \frac{d\eta\sigma^2 C}{\gamma} < r^2.$$

Define this event as \mathcal{E}_2 .

Denote $H = \nabla^2 h(0)$, we have that,

$$\begin{aligned} & \left| \mathbb{E}[h(\tilde{y}_k)] - \mathbb{E}[(\tilde{y}_k)^T H \tilde{y}_k] \right| \\ & = \left| \mathbb{E}[h(\tilde{y}_k) \mid \mathcal{E}_2] \mathbb{P}(\mathcal{E}_2) - \mathbb{E}[(\tilde{y}_k)^T H \tilde{y}_k] + \mathbb{E}[h(\tilde{y}_k) \mid \mathcal{E}_2^c] \mathbb{P}(\mathcal{E}_2^c) \right| \\ & \leq \delta M + \left| \mathbb{E}[h(\tilde{y}_k) \mid \mathcal{E}_2] \mathbb{P}(\mathcal{E}_2) - \mathbb{E}[(\tilde{y}_k)^T H \tilde{y}_k] \right| \\ & \leq \delta M + \rho \left(\frac{\eta d\sigma^2 C}{\gamma} \right)^{3/2} + \mathbb{E}[(\tilde{y}_k)^T H \tilde{y}_k \mid \mathcal{E}_2^c] \end{aligned}$$

Combining the both and we have that

$$\left| \mathbb{E}[h(y_k)] - \mathbb{E}[(\tilde{y}_k)^T H \tilde{y}_k] \right| \leq 4 \frac{\Delta\rho C}{\gamma^2} \eta d\sigma^2 + \rho \left(\frac{\eta d\sigma^2 C}{\gamma} \right)^{3/2} + 2\delta M + \mathbb{E}[(\tilde{y}_k)^T H \tilde{y}_k \mid \mathcal{E}_2^c].$$

Here the covariance of \tilde{y}_k , denoted as Σ_k satisfies that

$$\Sigma_{k+1} = (\mathcal{I} - \eta H)^2 \Sigma_k + \sigma^2 \eta^2 \mathcal{I}.$$

Therefore

$$\begin{aligned} \Sigma_k - \eta\sigma^2(2\eta H - \eta^2 H^2)^{-1} &= (\mathcal{I} - \eta H)^2 (\Sigma_{k-1} - \eta\sigma^2(2\eta H - \eta^2 H^2)^{-1}). \\ \Sigma_k &= \sigma^2(2H - \eta H^2)^{-1} (\mathcal{I} - (\mathcal{I} - \eta H)^{2k}). \end{aligned}$$

Hence assuming the eigenvalues of H is $\gamma_1, \dots, \gamma_d$

$$\mathbb{E}[(\tilde{y}_k)^T H \tilde{y}_k] = \text{Tr}(\Sigma_k H) = \eta\sigma^2 \sum_{i=1}^d \frac{1}{2 - \eta\gamma_i} (1 - (1 - \eta\gamma_i)^{2k}).$$

When $t \geq \frac{1}{\eta\gamma_i}$, $\eta\gamma_i < 1/2$, it holds that

$$\begin{aligned} & \left| \eta\sigma^2 \frac{1}{2 - \eta\gamma_i} (1 - (1 - \eta\gamma_i)^{2k}) - \eta\sigma^2/2 \right| \\ &= \eta\sigma^2 \frac{(1 - (1 - \eta\gamma_i)^{2k})}{2 - \eta\gamma_i} - \eta\sigma^2/2 \\ &\leq \eta\sigma^2 \left(\frac{1}{2 - \eta\gamma_i} - \frac{1}{2} \right) \\ &\leq \eta^2\sigma^2\gamma_i/2. \end{aligned}$$

Hence

$$\left| \mathbb{E}[(\tilde{y}_k)^T H \tilde{y}_k] - d\eta\sigma^2/2 \right| \leq \text{Tr}(H)\eta^2\sigma^2/2.$$

Further, let $u_k = \Sigma_k^{-1/2}\tilde{y}_k$, under \mathcal{E}_2^c , we have that

$$\|u_k\|_2^2 \geq \lambda_{\min}(\Sigma_k^{-1})\|\tilde{y}_k\|_2^2 = \lambda_{\min}((2H - \eta H^2)(\mathcal{I} - (\mathcal{I} - \eta H)^{2k})^{-1})\|\tilde{y}_k\|_2^2/\sigma^2 \geq d\sigma^2 C.$$

As u_k is isometric Gaussian,

$$\begin{aligned} \mathbb{E}[(\tilde{y}_k)^T H \tilde{y}_k \mid \mathcal{E}_2^c] &\leq \mathbb{E}[u_k^T (\Sigma_k^{1/2})^T H \Sigma_k^{1/2} u_k \mid \|u_k\|_2^2 \geq d\sigma^2 C] \\ &= \mathbb{E}[u_k^T (\Sigma_k^{1/2})^T H \Sigma_k^{1/2} u_k] \frac{\mathbb{E}[\|u_k\|_2^2 \mid \|u_k\|_2^2 \geq d\sigma^2 C]}{\mathbb{E}[\|u_k\|_2^2]} \\ &\leq d\eta\sigma^2 \frac{\mathbb{E}[\|u_k\|_2^2 \mid \|u_k\|_2^2 \geq d\sigma^2 C]}{\mathbb{E}[\|u_k\|_2^2]} \end{aligned}$$

Plugging in the density function of $\|u_k\|_2$, we have that

$$\frac{\mathbb{E}[\|u_k\|_2^2 \mid \|u_k\|_2^2 \geq d\sigma^2 C]}{\mathbb{E}[\|u_k\|_2^2]} = \frac{\int_{\sqrt{dC}\sigma}^{\infty} r^{d+1} e^{-r^2/(2\sigma^2)} dr}{\int_0^{\infty} r^{d+1} e^{-r^2/(2\sigma^2)} dr}$$

Let $r' = \sqrt{\frac{d}{d+1}}r$, then

$$\begin{aligned} \int_{\sqrt{dC}\sigma}^{\infty} r^{d+1} e^{-r^2/\sigma^2} dr &= \left(\frac{d+1}{d}\right)^{\frac{d+2}{2}} \int_{d\sigma^2 C}^{\infty} r'^{d+1} e^{-(r')^2/(2d\sigma^2)} dr' \\ &\leq 4 \int_{\sqrt{dC}\sigma}^{\infty} r'^{d+1} e^{-(r')^2/(2\sigma^2)} e^{-(r')^2/(2d\sigma^2)} dr' \\ &\leq 4e^{-C/2} \int_0^{\infty} r^{d+1} e^{-r^2/(2\sigma^2)} dr. \end{aligned}$$

Hence, we have that

$$\mathbb{E}[(\tilde{y}_k)^T H \tilde{y}_k \mid \mathcal{E}_2^c] \leq 4e^{-C/2} d\eta\sigma^2 \leq \delta d\eta\sigma^2/2.$$

Putting together, we have that,

$$\left| \mathbb{E}[h(\tilde{y}_k)] - \eta\sigma^2 d/2 \right| \leq \eta^2\sigma^2 \text{Tr}(H) + \frac{\Delta\rho C}{\gamma^2} d\eta\sigma^2 + \rho \left(\frac{d\eta\sigma^2 C}{\gamma} \right)^{3/2} + 2\delta M + \delta\eta\sigma^2 d/2.$$

The proof is then complete. \square

We will now state the complete version of Theorem 3.4.

Assumption 7 (Sufficient Small Learning Rate). *We will assume the following for constant $\delta \in (0, 1]$ and learning rate η :*

1. $\eta < 1/(2\gamma_{\max})$.
2. $\eta \leq \gamma^3/(1600\rho^2\sigma^2d\log(8\gamma T/\delta))$.
3. $10\frac{\sqrt{\eta}\sigma}{\sqrt{\gamma}}\sqrt{d\log(8\gamma T/\delta)} + 400\eta\rho\sigma^2d\log(8\gamma T/\delta)/\gamma^2 \leq r$.

Theorem A.30 (Complete version of Theorem 3.4). *If a loss L is a river valley (Definition 3.1) and satisfies Assumptions 3 and 4, for any constants $\delta \in (0, 1)$ and $T > 1/\gamma$, for sufficiently small learning rate η satisfying Assumption 7, there exists a time shift T_0 depending on w and η , the SGD iterates (defined in Equation (4)) with $\eta_k = \eta$ satisfies that for any integer $k \in [1/\eta\gamma, T_{\max}/\eta]$, there exists a $\tilde{t} \in [(1 - \epsilon_t)\eta k, (1 + \epsilon_t)\eta k]$ satisfying that,*

$$\mathbb{E}[L(\tilde{w}(k))] - L(x(T_0 + \tilde{t})) = (d - 1)\eta\sigma^2/2 + \epsilon_L$$

where $\epsilon_t = 4\eta\gamma_{\text{flat}}$ and $|\epsilon_L| \leq \tau\eta^2\sigma^2 + \rho(Cd\eta\sigma^2/\gamma)^{3/2} + C\kappa'd\eta\sigma^2 + \delta(2M + \eta\sigma^2d) \ll (d - 1)\eta\sigma^2$ with $C = 200\log(64\gamma T/\delta)$.

Proof. By Lemma A.26, we can write

$$L(w) = h(w - \Phi(w)) + L(\Phi(w)).$$

Hence we can separate the dynamics of Equation (4) into two parts, namely $w = \Phi(w) + (w - \Phi(w))$. It is easy to check that when constrained on range of P_S , $h(y)$ satisfies Assumption 6. Hence, we can use Lemma A.29 to control $h(w_k - \Phi(w_k))$. For $\Phi(w_k)$, the iterates is running a gradient descent with learning rate η on \mathcal{M} and we can use proof analogous to the proof of Theorem 3.3 to show that if $\Phi(w_k) = x(\tilde{T}(k, \eta))$, then there exists T_0 , such that

$$\tilde{T}(k, \eta) \in [T_0 + (1 - 4\eta\gamma_{\text{flat}})\eta k, T_0 + (1 + 4\eta\gamma_{\text{flat}})\eta k].$$

This completes the proof. \square

A.7 PROOF OF THEOREM 3.5

We will first state the complete version of Theorem 3.5.

Theorem A.31. *Under the setting of Theorem A.30, the SGD iterates (defined in Equation (4)) with the learning rate schedule defined in Equation (5) satisfies that for any integer $k \in [k_s, 1.1k_s]$, there exists a $\tilde{t} \in [(1 - \epsilon_t)T(t), (1 + \epsilon_t)T(t)]$ satisfying that,*

$$\mathbb{E}[L(\tilde{w}(k))] - L(x(T_0 + \tilde{t})) \leq (d - 1)\eta_k\sigma^2/2 + \epsilon_L$$

$$\text{with } T(t) = T + \sum_{i=k_s}^k \eta_i.$$

Proof. The proof is analogous to Theorem A.30 and Lemma A.29. We will omit the detail derivation and only focus on deriving the variance of corresponding \tilde{y}_k .

$$\tilde{y}(k + 1) = \tilde{y}_k - \eta_k H \tilde{y}_k - \eta_k g_k, w(0) = 0, \mathbf{g}_k \sim \mathcal{N}(0, \sigma^2 \mathcal{I}), \tilde{y}(0) = 0.$$

Here the covariance of \tilde{y}_k , denoted as Σ_k satisfies that

$$\Sigma_{k+1} = (\mathcal{I} - \eta_k H)^2 \Sigma_k + \sigma^2 \eta_k^2 \mathcal{I}.$$

If we consider i -th eigenvector of H as v_i , and denote $\sigma_{k,i} = v_i^\top \Sigma v_i$.

Analogous to the proof of Theorem A.30, $\left| \sigma_{k_s,i} - \frac{\eta\sigma^2}{\gamma_i} \right| \leq \frac{4\eta^2\sigma^2}{\gamma_i}$.

We further have that

$$\sigma_{k_s+r+1,i} = (1 - \frac{\eta}{2 + r\eta\gamma}\gamma_i)^2 \sigma_{k_s+r,i} + \sigma^2 \frac{\eta^2}{(2 + r\eta\gamma)^2}.$$

Then by induction, we can prove that for $r \geq 0$

$$\sigma_{k_s+r+1,i} \leq \frac{\sigma^2}{\gamma_i} \frac{\eta}{2 + r\eta\gamma} + \frac{4\eta^2\sigma^2}{\gamma_i} = \frac{\sigma^2}{\gamma_i} \eta_{t_s+r+1} + \frac{4\eta^2\sigma^2}{\gamma_i}.$$

The rest follows the proof of Theorem A.30. \square

A.8 PROOF OF LEMMA 4.1 AND THEOREM A.33

In this section, we will denote $\frac{\exp(\Theta_{i,j})}{\sum_{j=1}^m \exp(\Theta_{i,j})}$ as $\mathcal{Q}_{i,j}$

Lemma A.32. *The loss defined L in Equation (6) satisfies that*

$$\begin{aligned} (\nabla L(\Theta))_{(i,j)} &= \mathcal{P}_{i,j} - \mathcal{Q}_{i,j}, \\ (\nabla^2 L(\Theta))_{(i,j),(i',j')} &= \mathbf{1}(i = i')(\mathcal{Q}_{i,j} \mathbf{1}(j = j') - \mathcal{Q}_{i,j} \mathcal{Q}_{i,j'}). \end{aligned}$$

Proof. The loss satisfies that

$$L(\Theta) = \sum_{i=1}^n \left(\sum_{j=1}^m \mathcal{P}_{i,j} \Theta_{i,j} \right) - \log \left(\sum_{j'=1}^m \mathcal{P}_{i,j'} \right).$$

Hence,

$$(\nabla L(\Theta))_{(i,j)} = \mathcal{P}_{i,j} - \mathcal{Q}_{i,j}.$$

Taking differentiation for another time yields the desired result. \square

Proof of Lemma 4.1. This can be done by directly summing diagonal entries in Lemma A.32. \square

Assumption 8. *We will assume there exists constant γ and positive integer $n' < n$ such that \mathcal{P} satisfies the following assumption,*

1. *For any $i \leq n'$, $\forall j, \mathcal{P}_{i,j} > 8\gamma$.*
2. *For any $i > n'$, there exists $j_i, \mathcal{P}_{i,j_i} > 1 - \gamma$.*

Theorem A.33. *Under Assumption 8, a generalized river with dimension $n'm + (n - n')$ exists in the loss landscape defined by L in Equation (6).*

Proof. According to Lemma A.32, the Hessian for L is block-diagonal. Now fixing a city i , we will analyze the eigenvalue distribution in this block. Let $q = [\mathcal{Q}_{i,j'}]_{j' \in [m]}$, then this block is $\text{diag}(q) - qq^T$.

For all non-zero eigenvalue λ for this block, there exists v such that

$$\text{diag}(q)v - q^T v q = \lambda v.$$

Hence, we have that

$$v_j = \frac{q_j q^T v}{q_j - \lambda}$$

This implies $\sum_{j=1}^m \frac{q_j^2}{q_j - \lambda} = 1$. We then have $\lambda \geq 0$ and there exists only one eigenvector corresponding to $\lambda = 0$. For the rest nonzero eigenvalue, we have that $\lambda > \min q_i$.

Now if we consider the manifold \mathcal{M} defined as

$$\mathcal{M} = \{\Theta \mid \forall i \leq n', \mathcal{Q}_{i,j} = \mathcal{P}_{i,j}; \forall i \geq n', \mathcal{Q}_{i,j_i} > 1 - \gamma\}.$$

Then for all $\Theta \in \mathcal{M}$, we have that the gradient is zero for all dimensions (i, j) with $i \leq n'$. Further, we know all the nonzero eigenvalues for these dimensions are at least 8γ by Assumption 8. For the rest of dimensions (i, j) with $i > n'$, by Lemma 4.1, the largest eigenvalue is bounded by $1 - (1 - \gamma)^2 < 2\gamma$. This shows that the gradient falls in the eigenspace spanned by the last $n'm + (n - n')$ eigenvectors, which concludes the proof. \square

A.9 TECHNICAL LEMMA

Lemma A.34. *If a function $F(t)$ satisfies that*

$$\frac{dF(t)}{dt} \leq -AF(t),$$

then $F(t) \leq e^{-At}F(0)$.

Proof of Lemma A.34. Consider $G(t) = F(t)e^{At}$, then

$$dG(t) = e^{At}dF(t) + Ae^{At}F(t) \leq 0.$$

Hence $G(t) \leq G(0)$. □

Lemma A.35. *If a random vector $g \sim \mathcal{N}(0, \Sigma)$ and $\delta \in (0, 1)$, then it holds that*

$$\mathbb{P}(\|g\|_2 \geq 2\sqrt{\text{Tr}(\Sigma)}\sqrt{\log(2/\delta)}) \leq \delta$$

Proof of Lemma A.35. Assume $\Sigma = Q\Lambda^2Q^T$ with Q being an orthonormal matrix and Λ being diagonal with diagonal λ_i for $i \in [d]$, further let g' being a standard gaussian random vector, then g follows the same distribution as that of $\Lambda Q^T g'$, which is further identical to $\Lambda g'$.

$$\begin{aligned} & \mathbb{P}(\|g\|_2 \geq C) \\ &= \mathbb{P}(\|\Lambda g'\|_2 \geq C) \\ &= \mathbb{P}\left(\sum_{i=1}^d \Lambda_i^2 (g'_i)^2 \geq C^2\right) \\ &\leq \mathbb{E}\left[\exp\left(t \sum_{i=1}^d \Lambda_i^2 (g'_i)^2 - tC^2\right)\right]. \end{aligned}$$

It is well known that the moment-generating function of $(g'_i)^2$ is

$$E[\exp(t\Lambda_i^2(g'_i)^2)] = \frac{1}{\sqrt{1 - 2t\Lambda_i^2}}.$$

Hence

$$\begin{aligned} \mathbb{P}(\|g\|_2 \geq C) &\leq e^{-tC^2} \prod_{i=1}^d \frac{1}{\sqrt{1 - 2t\Lambda_i^2}} \\ &\leq \frac{e^{-tC^2}}{\sqrt{1 - 2t\text{Tr}(\Sigma)}}. \end{aligned}$$

With $t = \frac{1}{4\text{Tr}(\Sigma)}$, it holds that

$$\mathbb{P}(\|g\|_2 \geq C) \leq 2e^{-\frac{C^2}{4\text{Tr}(\Sigma)}}.$$

This concludes the proof. □

Lemma A.36 (Doob's Inequality). *Let X_1, \dots, X_n as a positive submartingale adapted to filtration $\mathcal{F}_1, \dots, \mathcal{F}_n$, which means $X_i \leq \mathbb{E}[X_{i+1} \mid \mathcal{F}_i]$, then*

$$\mathbb{P}(\sup_{i \leq n} X_i > C) \leq \frac{\mathbb{E}[X_n]}{C}.$$

Model	Hidden Dim	Intermediate Dim	Num Layers	Num Heads	Peak LR
0.1B LLaMa	768	3072	12	12	6e-4
0.3B LLaMa	1024	2048	24	16	6e-4
0.6B LLaMa	1536	6144	24	32	4e-4
1.2B LLaMa	2048	8096	16	32	4e-4
0.1B GPT-2	768	3072	12	12	6e-4

Table 1: Specifications for Different Sizes of LLaMa Models

B OMITTED EXPERIMENTS DETAILS

We train LLaMA models with 4 parameter sizes using the Levanter framework for our study on *WSD-S*. For our theoretical study, we pretrain a 124M GPT-2 using the nanoGPT framework with a learning rate 6e-4 and train it with a batch size of 0.5M for 100k steps with warmup steps of 2k.

We hereby provide all the hyperparameters we used for the LLaMA and GPT-2 models training.

We decay the model for the last 10% of the training runs with one exception for 0.3B model using *WSD* method near 25k steps to avoid loss spikes. We outline the decaying and resuming point (the unit is 1k steps) we choose here:

Model	1st Decay Starts/Resume	2nd Decay Starts/Resume	3rd Decay Starts
0.1B LLaMa	11.25 / 12.5	22.5 / 25	48.75/ 53.75
0.3B LLaMa	11.25 / 12.5	22.5 / 25	48.75/ 53.75
0.6B LLaMa	11.25 / 12.5	22.5 / 25	48.75/ 53.75
1.2B LLaMa	11.25 /12.5	22.5 / 25	48.75/ 53.75

Table 2: Specifications for Decaying Steps for *WSD-S* Method

Model	1st Decay Starts/Ends	2nd Decay Starts/Ends	3rd Decay Starts	Total Steps
0.1B LLaMa	11.25 / 12.5	22.5 / 25	45/ 50	53.75
0.3B LLaMa	11.25 / 12.5	22 / 25	45/ 50	54
0.6B LLaMa	11.25 / 12.5	22.5 / 25	45/ 50	53.75
1.2B LLaMa	11.25 /12.5	22.5 / 25	45/ 50	53.75

Table 3: Specifications for Decaying Steps for *WSD* Method